

*Dynamical responses to external stimuli
for both cases of excitatory and inhibitory
synchronization in a complex neuronal
network*

Sang-Yoon Kim & Woochang Lim

Cognitive Neurodynamics

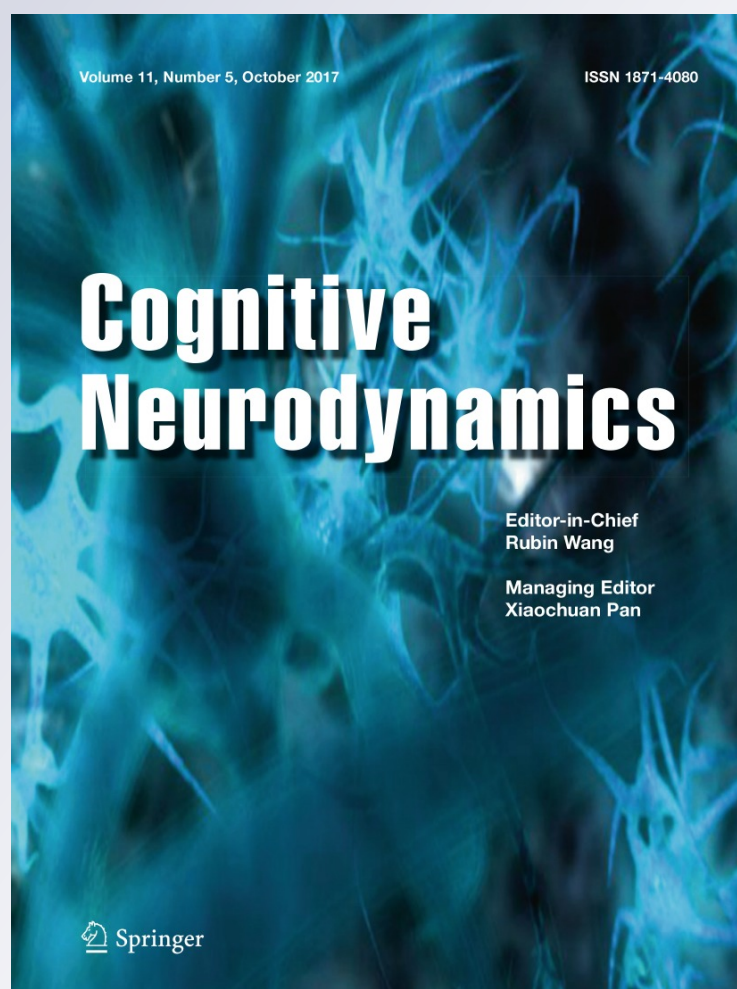
ISSN 1871-4080

Volume 11

Number 5

Cogn Neurodyn (2017) 11:395-413

DOI 10.1007/s11571-017-9441-5



Your article is protected by copyright and all rights are held exclusively by Springer Science +Business Media Dordrecht. This e-offprint is for personal use only and shall not be self-archived in electronic repositories. If you wish to self-archive your article, please use the accepted manuscript version for posting on your own website. You may further deposit the accepted manuscript version in any repository, provided it is only made publicly available 12 months after official publication or later and provided acknowledgement is given to the original source of publication and a link is inserted to the published article on Springer's website. The link must be accompanied by the following text: "The final publication is available at link.springer.com".

RESEARCH ARTICLE

Dynamical responses to external stimuli for both cases of excitatory and inhibitory synchronization in a complex neuronal network

Sang-Yoon Kim¹ · Woochang Lim¹

Received: 23 February 2017 / Revised: 8 May 2017 / Accepted: 17 May 2017 / Published online: 10 June 2017
© Springer Science+Business Media Dordrecht 2017

Abstract For studying how dynamical responses to external stimuli depend on the synaptic-coupling type, we consider two types of excitatory and inhibitory synchronization (i.e., synchronization via synaptic excitation and inhibition) in complex small-world networks of excitatory regular spiking (RS) pyramidal neurons and inhibitory fast spiking (FS) interneurons. For both cases of excitatory and inhibitory synchronization, effects of synaptic couplings on dynamical responses to external time-periodic stimuli $S(t)$ (applied to a fraction of neurons) are investigated by varying the driving amplitude A of $S(t)$. Stimulated neurons are phase-locked to external stimuli for both cases of excitatory and inhibitory couplings. On the other hand, the stimulation effect on non-stimulated neurons depends on the type of synaptic coupling. The external stimulus $S(t)$ makes a constructive effect on excitatory non-stimulated RS neurons (i.e., it causes external phase lockings in the non-stimulated sub-population), while $S(t)$ makes a destructive effect on inhibitory non-stimulated FS interneurons (i.e., it breaks up original inhibitory synchronization in the non-stimulated sub-population). As results of these different effects of $S(t)$, the type and degree of dynamical response (e.g., synchronization enhancement or suppression), characterized by the dynamical response factor D_f (given by the ratio of synchronization degree in the presence and absence of stimulus), are found to vary in

a distinctly different way, depending on the synaptic-coupling type. Furthermore, we also measure the matching degree between the dynamics of the two sub-populations of stimulated and non-stimulated neurons in terms of a “cross-correlation” measure M_c . With increasing A , based on M_c , we discuss the cross-correlations between the two sub-populations, affecting the dynamical responses to $S(t)$.

Keywords Excitatory synchronization · Inhibitory synchronization · External time-periodic stimulus · Dynamical response factor · Cross-correlation measure · Synchronization enhancement · Synchronization suppression

Introduction

Recently, much attention has been paid to brain rhythms in health and diseases (Buzsáki 2006; Traub and Whittington 2010). These brain rhythms emerge via synchronization between individual firings in neural circuits. This kind of neural synchronization may be used for efficient sensory and cognitive processing such as sensory perception, multisensory integration, selective attention, and memory formation (Wang 2003, 2010; Gray 1994), and it is also correlated with pathological rhythms associated with neural diseases (e.g., epileptic seizures and tremors in the Parkinson’s disease) (Traub and Whittington 2010; Hammond et al. 2007; Uhlhaas and Singer 2006). The brain receives natural sensory stimulation, and experimental electrical or magnetic stimulation in the neural system is used for analyzing the dynamical interactions between different brain areas. Responses to these external stimuli can provide crucial information about its dynamical properties. For example, the effects of periodic stimuli on

✉ Woochang Lim
wclim@icn.re.kr

Sang-Yoon Kim
sykim@icn.re.kr

¹ Institute for Computational Neuroscience and Department of Science Education, Daegu National University of Education, Daegu 42411, Korea

rhythmic biological activity were experimentally studied by applying rhythmic visual stimulus (Mathewson et al. 2012) and periodic auditory stimulation (Will and Berg 2007). Hence, it is of great importance to investigate how an external stimulus affects the neural synchronization in the brain. Techniques for controlling population synchronization have been proposed, which enables us to suppress or to enhance it. For examples, one technique is the external time-periodic stimulation (Ivanchenko et al. 2004; Batista et al. 2007; Viana et al. 2012; Batista et al. 2013), and the other one is the time-delayed feedback in the mean field (Batista et al. 2013; Rosenblum and Pikovsky 2004a, b; Batista et al. 2010). Synchronization suppression may be effective in suppressing pathological brain rhythms. Particularly, deep brain stimulation techniques have been used to suppress pathological rhythms in patients with neural diseases such as Parkinson's disease, essential tremor, and epilepsy (Hamani et al. 2006; Benabid et al. 2009; Milton and Jung 2003). For this technique, micro-electrodes are implanted in deep brain regions of patients, and then time-periodic electric signal or time-delayed feedback signals are injected for suppression of abnormal rhythms. On the other hand, synchronization enhancement may be useful for the cases of failures of cardiac or neural pacemakers (Rosenblum and Pikovsky 2004a) and encoding temporal features of the sound in auditory system (Joris et al. 1994).

Most of previous theoretical and computational works on control of population synchronization were focused on the case of excitatory-type couplings (Ivanchenko et al. 2004; Batista et al. 2007; Viana et al. 2012; Batista et al. 2013; Rosenblum and Pikovsky 2004a, b; Batista et al. 2010). To study how dynamical responses depend on the synaptic-coupling type (excitatory or inhibitory), we consider two types of excitatory and inhibitory population synchronization occurring via excitatory and inhibitory interactions. Neurons, constituting the population, may be suprathreshold or subthreshold. For the suprathreshold case, neurons may make spontaneous firings, while in the subthreshold case they can fire only with help of noise because they cannot fire spontaneously. For general cases of excitatory coupling, suprathreshold neurons exhibit full synchronization (i.e., all neurons fire like clock oscillators in each global cycle of the population rhythm) (Wang 2003). However, when the noise intensity passes a threshold, this type of full synchronization becomes broken up (i.e., a transition to desynchronization occurs) due to a destructive role of noise. On the other hand, for the case of inhibitory coupling, suprathreshold neurons show diverse types of population synchronizations such as full, partial and sparse (i.e., only a fraction of neurons fire intermittently and stochastically like Geiger counters in each global cycle of the population rhythm) synchronization,

depending on the values of the strength of inhibition coupling and the noise intensity (Kim and Lim 2015b). Unlike the suprathreshold case, noise may play a constructive role to stimulate coherence between noise-induced firings of subthreshold neurons. As a result, when passing a lower threshold of noise intensity, stochastic spike/burst full (sparse) synchronization was found to occur for the case of excitatory (inhibitory) subthreshold neurons (Lim and Kim 2007; Kim and Lim 2013; Kim et al. 2012; Lim and Kim 2011; Kim and Lim 2015a). However, when passing a higher threshold of noise intensity, transitions to desynchronization occurs due to a destructive role of noise. In this way, diverse population states emerge, depending on the coupling strength and the noise intensity. Here, for focusing on our purpose (i.e., investigation of dependence of dynamical responses on the synaptic-coupling type), we consider two simple types of excitatory and inhibitory full synchronization in complex networks of excitatory regular spiking (RS) suprathreshold pyramidal neurons and inhibitory fast spiking (FS) suprathreshold interneurons. In a real brain network, synaptic connections are known to have complex topology which is neither regular nor completely random (Sporns 2011; Buzsáki et al. 2004; Bullmore and Sporns 2009). As a complex network, we employ the Watts–Strogatz model for small-world networks which interpolates between regular lattice with high clustering and random graph with short path length (Watts and Strogatz 1998; Strogatz 2001; Watts 2003). We apply external time-periodic stimuli $S(t) [= A \sin(\omega_d t)]$ to a fraction of neurons for both cases of excitatory and inhibitory synchronization, and investigate their dynamical responses to $S(t)$ by changing the driving amplitude A for a fixed driving angular frequency ω_d . For describing collective behaviors in the whole population, we use an instantaneous whole-population spike rate (IWPSR) $R_w(t)$ which may be obtained from the raster plot of spikes where population synchronization may be well seen (Kim and Lim 2014). For the case of synchronization, $R_w(t)$ shows an oscillatory behavior, while it becomes nearly stationary in the case of desynchronization. We characterize dynamical responses to $S(t)$ in terms of a dynamical response factor D_f (given by the square root of the ratio of the variance of $R_w(t)$ in the presence and absence of stimulus). If D_f is larger than 1, then synchronization enhancement occurs; otherwise (i.e., $D_f < 1$), synchronization suppression takes place. For both cases of excitatory and inhibitory couplings, stimulated neurons are phase-locked to external stimuli $S(t)$. In contrast, the stimulation effect on non-stimulated neurons varies depending on the synaptic-coupling type. For the excitatory case, non-stimulated RS neurons are also phase-locked to external stimulus $S(t)$ thanks to a constructive effect of $S(t)$ (resulting from phase-attractive synaptic excitation). On the other hand, in the inhibitory case the original full

synchronization in the non-stimulated sub-population breaks up gradually with increasing A due to a destructive effect of $S(t)$ (coming from strong synaptic inhibition), and then a new type of sparse synchronization (where only some fraction of neurons fire in each global cycle of population rhythm) appears. As results of these different effects of $S(t)$, the type and degree of dynamical response (characterized by D_f) vary differently, depending on the type of synaptic interaction. For further analysis of dynamical response, we also decompose the whole population into two sub-populations of the stimulated and the non-stimulated neurons. Then, two instantaneous sub-population spike rates (ISPSRs) $R_s^{(1)}(t)$ and $R_s^{(2)}(t)$ [the superscript 1 (2) corresponds to the stimulated (non-stimulated) case] may be used to show collective behaviors in the two sub-populations of stimulated and non-stimulated neurons, respectively, and the matching degree between the dynamics of the stimulated and the non-stimulated sub-populations is measured in terms of a “cross-correlation” measure M_c between $R_s^{(1)}(t)$ and $R_s^{(2)}(t)$. M_c also varies with A in a distinctly different way, depending on the synaptic-coupling type, because of different effects of $S(t)$. Based on the cross-correlations between the two sub-populations (characterized by M_c), we also discuss the dynamical responses to $S(t)$.

This paper is organized as follows. In “[Small-world networks of excitatory RS pyramidal neurons and inhibitory FS interneurons](#)” section, we describe complex small-world networks of excitatory RS pyramidal neurons and inhibitory FS interneurons, and the governing equations for the population dynamics are given. Then, in “[Effects of synaptic-coupling type on dynamical responses to external time-periodic stimuli](#)” section we investigate the effects of synaptic couplings on dynamical responses to external time-periodic stimuli $S(t)$ for both excitatory and inhibitory cases. Finally, in “[Summary](#)” section a summary is given. Explanations on methods for characterization of synchronization in each of the stimulated and the non-stimulated sub-populations are also made in “[Appendix](#)”.

Small-world networks of excitatory RS pyramidal neurons and inhibitory FS interneurons

We consider two types of directed Watts–Strogatz small-world networks (SWNs) with N neurons equidistantly placed on a one-dimensional ring of radius $N/2\pi$; the first type of SWN consists of excitatory RS pyramidal neurons, while the second type of SWN is composed of inhibitory FS interneurons. The Watts–Strogatz SWN interpolates between a regular lattice with high clustering (corresponding to the case of $p = 0$) and a random graph with short average path length (corresponding to the case of

$p = 1$) via random uniform rewiring with the probability p (Watts and Strogatz 1998; Strogatz 2001; Watts 2003). For $p = 0$, we start with a directed regular ring lattice with N nodes where each node is coupled to its first M_{syn} neighbors ($M_{syn}/2$ on either side) via outward synapses, and rewire each outward connection uniformly at random over the whole ring with the probability p (without self-connections and duplicate connections). This Watts–Strogatz SWN model may be regarded as a cluster-friendly extension of the random network by reconciling the six degrees of separation (small-worldness) (Milgram 1967; Guare 1990) with the circle of friends (clustering). As elements in our neural networks, we choose the Izhikevich RS pyramidal neuron and FS interneuron models which are not only biologically plausible, but also computationally efficient (Izhikevich 2003, 2004, 2007, 2010).

The following Eqs. (1)–(8) govern the population dynamics in the SWNs:

$$C \frac{dv_i}{dt} = k(v_i - v_r)(v_i - v_t) - u_i + I_{DC} + D\xi_i - I_{syn,i} + S_i(t), \quad (1)$$

$$\frac{du_i}{dt} = a\{U(v_i) - u_i\}, \quad i = 1, \dots, N, \quad (2)$$

with the auxiliary after-spike resetting:

$$\text{if } v_i \geq v_p, \text{ then } v_i \leftarrow c \text{ and } u_i \leftarrow u_i + d, \quad (3)$$

where

$$U(v) = b(v - v_b) \text{ for the RS pyramidal neurons,} \quad (4)$$

$$= \begin{cases} 0 & \text{for } v < v_b \\ b(v - v_b)^3 & \text{for } v \geq v_b \end{cases} \text{ for the FS interneurons,} \quad (5)$$

$$I_{syn,i} = \frac{J}{d_i^{(in)}} \sum_{j=1, j \neq i}^N w_{ij} s_j(t) (v_i - V_{syn}), \quad (6)$$

$$s_j(t) = \sum_{f=1}^{F_j} E(t - t_f^{(j)} - \tau_l); \quad (7)$$

$$E(t) = \frac{1}{\tau_d - \tau_r} (e^{-t/\tau_d} - e^{-t/\tau_r}) \Theta(t),$$

$$S_i(t) = \alpha_i A \sin(\omega_d t). \quad (8)$$

Here, $v_i(t)$ and $u_i(t)$ are the state variables of the i th neuron at a time t which represent the membrane potential and the recovery current, respectively. These membrane potential and the recovery variable, $v_i(t)$ and $u_i(t)$, are reset according to Eq. (3) when $v_i(t)$ reaches its cutoff value v_p . C , v_r , and v_t in Eq. (1) are the membrane capacitance, the resting membrane potential, and the instantaneous threshold potential, respectively. The parameter values used in our computations are listed in Table 1. More details on the Izhikevich RS pyramidal neuron and FS interneuron

models, the external stimulus to each Izhikevich neuron, the synaptic currents, the external time-periodic stimulus to sub-populations of randomly-selected neurons, and the numerical method for integration of the governing equations are given in the following subsections.

Izhikevich RS pyramidal neuron and FS interneuron models

The Izhikevich model matches neuronal dynamics by tuning the parameters (k , a , b , c , d) instead of matching neuronal electrophysiology, unlike the Hodgkin-Huxley-type conductance-based models (Izhikevich 2003, 2004, 2007, 2010). The parameters k and b are related to the neuron's rheobase and input resistance, and a , c , and d are the recovery time constant, the after-spike reset value of v , and the after-spike jump value of u , respectively. Depending on the values of these parameters, the Izhikevich neuron model may exhibit 20 of the most prominent neuro-computational features of cortical neurons (Izhikevich 2003, 2004, 2007, 2010). Here, we use the parameter values for the RS pyramidal neurons and the FS interneurons in the layer 5 rat visual cortex, which are listed in the 1st and the 2nd items of Table 1 (Izhikevich 2007).

External stimulus to each Izhikevich neuron

Each Izhikevich neuron is stimulated by both a common DC current I_{DC} and an independent Gaussian white noise ξ_i [see the 3rd and the 4th terms in Eq. (1)]. The Gaussian white noise satisfies $\langle \xi_i(t) \rangle = 0$ and $\langle \xi_i(t) \xi_j(t') \rangle =$

$\delta_{ij} \delta(t - t')$, where $\langle \dots \rangle$ denotes the ensemble average. Here, the Gaussian noise ξ may be regarded as a parametric one which randomly perturbs the strength of the applied current I_{DC} , and its intensity is controlled by the parameter D . For $D = 0$, the Izhikevich RS pyramidal neurons exhibit the type-I excitability, while the Izhikevich FS interneurons show the type-II excitability (Izhikevich 2007). For the type-I case, a transition from a resting state to a spiking state occurs as I_{DC} passes a threshold via a saddle-node bifurcation on an invariant circle, and firing begins at arbitrarily low frequency (Izhikevich 2007; Hodgkin 1948; Izhikevich 2000). On the other hand, a type-II neuron exhibits a jump from a resting state to a spiking state through a subcritical Hopf bifurcation when passing a threshold by absorbing an unstable limit cycle born via fold limit cycle bifurcation and hence, the firing frequency begins from a non-zero value (Izhikevich 2007; Hodgkin 1948; Izhikevich 2000). The values of I_{DC} and D used in this paper are given in the 3rd item of Table 1.

Synaptic currents

The 5th term in Eq. (1) denotes the synaptic couplings of Izhikevich neurons. $I_{syn,i}$ of Eq. (6) represents the synaptic current injected into the i th neuron. The synaptic connectivity is given by the connection weight matrix $W(= \{w_{ij}\})$ where $w_{ij} = 1$ if the neuron j is presynaptic to the neuron i ; otherwise, $w_{ij} = 0$. Here, the synaptic connection is modeled in terms of the Watts–Strogatz SWN. The in-degree of the i th neuron, $d_i^{(in)}$ (i.e., the number of synaptic inputs to

Table 1 Parameter values used in our computations; units of the capacitance, the potential, the current, the time, and the angular frequency are pF, mV, pA, ms, and rad/ms respectively

(1)	Izhikevich RS pyramidal neurons (Izhikevich 2007)				
	$C = 100$	$v_r = -60$	$v_t = -40$	$v_p = 35$	$v_b = -60$
	$k = 0.7$	$a = 0.03$	$b = -2$	$c = -50$	$d = 100$
(2)	Izhikevich FS interneurons (Izhikevich 2007)				
	$C = 20$	$v_r = -55$	$v_t = -40$	$v_p = 25$	$v_b = -55$
	$k = 1$	$a = 0.2$	$b = 0.025$	$c = -45$	$d = 0$
(3)	External common stimulus to Izhikevich neurons				
	$I_{DC} = 70$	$D = 1$ (RS pyramidal neuron)			
	$I_{DC} = 1500$	$D = 50$ (FS interneuron)			
(4)	Excitatory AMPA and inhibitory GABAergic synapses (Brunel and Wang 2003)				
	$\tau_l = 1$	$\tau_r = 0.5$	$\tau_d = 2$	$V_{syn} = 0$ (excitatory AMPA synapse)	
	$\tau_l = 1$	$\tau_r = 0.5$	$\tau_d = 5$	$V_{syn} = -80$ (inhibitory GABAergic synapse)	
(5)	Synaptic connections between neurons				
	$M_{syn} = 50$ and $p = 0.2$ (Watts–Strogatz SWN)				
	$J = 15$ (RS pyramidal neurons)				
	$J = 100$ (FS interneurons)				
(6)	External time-periodic stimulus to Izhikevich neurons				
	A : Varying				
	$\omega_d = 0.048$ (RS pyramidal neurons)				
	$\omega_d = 1.26$ (FS interneurons)				

the neuron i) is given by $d_i^{(in)} = \sum_{j=1, (j \neq i)}^N w_{ij}$. For this case, the average number of synaptic inputs per neuron is given by $M_{syn} = \frac{1}{N} \sum_{i=1}^N d_i^{(in)}$.

The fraction of open synaptic ion channels at time t is denoted by $s(t)$. The time course of $s_j(t)$ of the j th neuron is given by a sum of delayed double-exponential functions $E(t - t_f^{(j)} - \tau_l)$ [see Eq. (7)], where τ_l is the synaptic delay, and $t_f^{(j)}$ and F_j are the f th spiking time and the total number of spikes of the j th neuron (which occur until time t), respectively. Here, $E(t)$ [which corresponds to contribution of a presynaptic spike occurring at time 0 to $s(t)$ in the absence of synaptic delay] is controlled by the two synaptic time constants: synaptic rise time τ_r and decay time τ_d , and $\Theta(t)$ is the Heaviside step function: $\Theta(t) = 1$ for $t \geq 0$ and 0 for $t < 0$. The synaptic coupling strength is controlled by the parameter J , and V_{syn} is the synaptic reversal potential. For both the excitatory AMPA synapse and the inhibitory GABAergic synapse (involving the GABA_A receptors), the values of τ_l , τ_r , τ_d , and V_{syn} are listed in the 4th item of Table 1 (Brunel and Wang 2003).

External time-periodic stimulus to sub-populations of randomly-selected neurons

The last term in Eq. (1) represents the external time-periodic stimulus to the i th neuron, $S_i(t)$, the explicit form of which is given in Eq. (8). If stimulus is applied to the i th neuron, $\alpha_i = 1$; otherwise, $\alpha_i = 0$ (In the absence of external stimulus, $\alpha_i = 0$ for all i). The driving angular frequency of the stimulus is ω_d , and its amplitude is A . We apply $S_i(t)$ to sub-groups of randomly-chosen $N_s (= 50)$ RS pyramidal neurons and FS interneurons, respectively.

Numerical method for integration

Numerical integration of stochastic differential Eqs. (1)–(8) is done by employing the Heun method (San Miguel and Toral 2000) with the time step $\Delta t = 0.01$ ms. For each realization of the stochastic process, we choose random initial points $[v_i(0), u_i(0)]$ for the i th ($i = 1, \dots, N$) RS pyramidal neuron and FS interneuron with uniform probability in the range of $v_i(0) \in (-50, -45)$ and $u_i(0) \in (10, 15)$.

Effects of synaptic-coupling type on dynamical responses to external time-periodic stimuli

In this section, we study the effects of synaptic-coupling type on dynamical responses to external time-periodic stimuli $S(t)$ in the Watts–Strogatz SWN with the average

number of synaptic inputs $M_{syn} = 50$ and the rewiring probability $p = 0.2$. Both the excitatory and the inhibitory cases are investigated by varying the driving amplitude A for a fixed driving angular frequency ω_d .

Dynamical response of excitatory synchronization to an external time-periodic stimulus

We consider an excitatory Watts–Strogatz SWN composed of $N (= 10^3)$ Izhikevich RS pyramidal neurons. Figure 1a shows a plot of the firing frequency f versus the external DC current I_{DC} for a single Izhikevich RS neuron in the absence of noise ($D = 0$). This Izhikevich RS neuron exhibits type-I excitability for $I_{DC} > 51$ because its frequency may be arbitrarily small (Izhikevich 2007; Hodgkin 1948; Izhikevich 2000). Here, we consider a suprathreshold case of $I_{DC} = 70$ in the presence of noise with its intensity $D = 1$ for which a time series of the membrane potential v with an oscillating frequency $f \simeq 7.0$ Hz is shown in Fig. 1b. We set the coupling strength as $J = 15$. Spike synchronization is well seen in the raster plot of spikes in

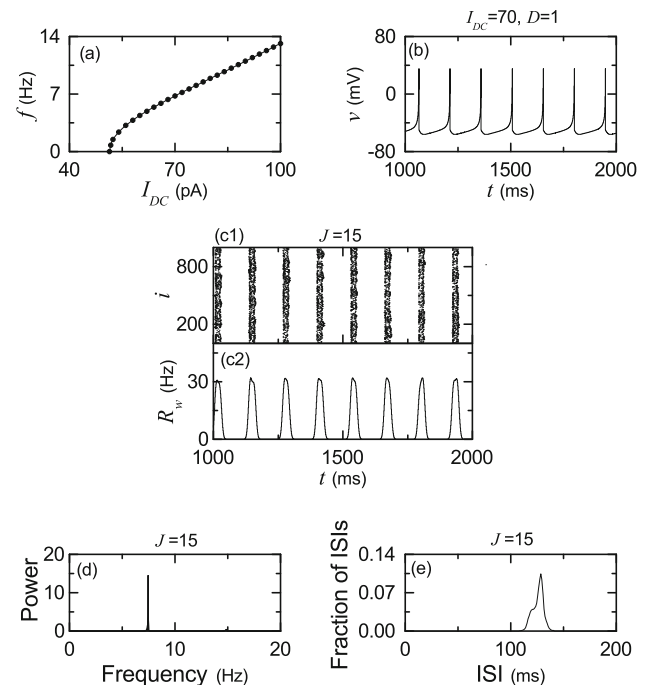


Fig. 1 Excitatory synchronization in the Watts–Strogatz SWN of $N (= 10^3)$ Izhikevich RS pyramidal neurons for $M_{syn} = 50$ and $p = 0.2$. Single Izhikevich RS pyramidal neuron: **a** plot of the mean firing rate f versus the external DC current I_{DC} for $D = 0$ and **b** time series of the membrane potential v for $I_{DC} = 70$ and $D = 1$. Coupled Izhikevich RS pyramidal neurons for $I_{DC} = 70$, $D = 1$, and $J = 15$: **c1** raster plot of spikes, **c2** plot of the instantaneous whole-population spike rate (IWPSR) kernel estimate $R_w(t)$ versus t , **d** one-sided power spectrum of $\Delta R_w(t) [= R_w(t) - \overline{R_w(t)}]$ (the *overbar* represents the time average) with mean-squared amplitude normalization, and **e** inter-spike interval (ISI) histogram

Fig. 1c1. “Stripes” (composed of synchronized spikes) appear regularly. All Izhikevich RS neurons fire synchronously in each stripe, and hence full synchronization occurs. For this synchronous case, an oscillating IWPSR (instantaneous whole-population spike rate) $R_w(t)$ appears. To obtain a smooth IWPSR, we employ the kernel density estimation (kernel smoother) (Shimazaki and Shinomoto 2010). Each spike in the raster plot is convoluted (or blurred) with a kernel function $K_h(t)$ to obtain a smooth estimate of IWPSR $R_w(t)$:

$$R_w(t) = \frac{1}{N} \sum_{i=1}^N \sum_{s=1}^{n_i} K_h(t - t_s^{(i)}), \quad (9)$$

where $t_s^{(i)}$ is the s th spiking time of the i th neuron, n_i is the total number of spikes for the i th neuron, and we use a Gaussian kernel function of band width h :

$$K_h(t) = \frac{1}{\sqrt{2\pi}h} e^{-t^2/2h^2}, \quad -\infty < t < \infty. \quad (10)$$

Figure 1c2 shows a regularly-oscillating IWPSR kernel estimate $R_w(t)$. Hereafter, the band width of the Gaussian kernel estimate for each IWPSR $R_w(t)$ is 7 ms for the excitatory case and 0.5 ms for the inhibitory case. The population frequency $f_p (\simeq 7.6 \text{ Hz})$ of $R_w(t)$ may be obtained from the peak in the power spectrum of $\Delta R_w(t) [= R_w(t) - \overline{R_w(t)}]$ (the overline represents the time average), which is shown in Fig. 1d. Throughout the paper, each power spectrum is obtained via 30 realizations [2¹⁶ (= 65536) data points are used in each realization]. For analysis of individual spiking behaviors, an inter-spike interval (ISI) histogram is given in Fig. 1e. Hereafter, each ISI histogram is obtained through 30 realizations (5 × 10⁷ ISIs are used in each realization) and the bin size for the histogram is 0.5 ms. The ensemble-averaged ISI $\langle ISI \rangle$ ($\langle \cdots \rangle$ denotes an ensemble average) is 131.6 ms, and hence the ensemble-averaged mean firing rate (MFR) $\langle f_i \rangle$ of individual neurons (f_i is the MFR of the i th neuron and $\langle f_i \rangle$ corresponds to the reciprocal of $\langle ISI \rangle$) is 7.6 Hz. For the case of full synchronization, $f_p = \langle f_i \rangle$, in contrast to the case of sparse synchronization where f_p is larger than $\langle f_i \rangle$ due to stochastic spike skipping of individual neurons (Brunel and Hakim 2008; Kim and Lim 2015b).

We apply an external time-periodic AC stimulus $S(t)$ to a sub-population of $N_s (= 50)$ randomly-selected Izhikevich RS pyramidal neurons by fixing the driving angular frequency as $\omega_d (= 2\pi f_d) = 0.048 \text{ rad/ms}$ ($f_d = \langle f_i \rangle = 7.6 \text{ Hz}$), and investigate the dynamical response of the above full synchronization for $J = 15$ by varying the driving amplitude A . Figure 2a1–a8 show raster plots of spikes for various values of A . Their corresponding IWPSR kernel estimates $R_w(t)$ are shown in Fig. 2b1–b8, and the

power spectra of $\Delta R_w(t)$ are also given in Fig. 2e1–e8. Population synchronization may be well seen in these raster plots of spikes. For a synchronous case, the IWPSR kernel estimates $R_w(t)$ exhibits an oscillating behavior. In addition, times series of individual membrane potentials $v_5(t)$ and $v_{20}(t)$ of the stimulated 5th and the non-stimulated 20th RS neurons are also given in Fig. 2c1–c8 and 2d1–d8, respectively. Then, the type and degree of dynamical response may be characterized in terms of a dynamical response factor D_f (Rosenblum and Pikovsky 2004a, b):

$$D_f = \sqrt{\frac{\text{Var}(R_w^{(A)})}{\text{Var}(R_w^{(0)})}}, \quad (11)$$

where $\text{Var}(R_w^{(A)})$ and $\text{Var}(R_w^{(0)})$ represent the variances of the IWPSR kernel estimate $R_w(t)$ in the presence and absence of stimulus, respectively. If the dynamical response factor D_f is larger than 1, then synchronization enhancement occurs; otherwise (i.e., $D_f < 1$), synchronization suppression takes place. Figure 2f shows a plot of $\langle D_f \rangle_r$ versus A . Here, $\langle \cdots \rangle_r$ denotes an average over 30 realizations, and averaging time for D_f in each realization is $3 \times 10^4 \text{ ms}$. Three stages are found to appear. Synchronization enhancement ($\langle D_f \rangle_r > 1$), synchronization suppression ($\langle D_f \rangle_r < 1$), and synchronization enhancement (i.e., increase in $\langle D_f \rangle_r$ from 1) occur in the 1st (I) stage ($0 < A < A_1^*$), the 2nd (II) stage ($A_1^* < A < A_2^*$), and the 3rd (III) stage ($A > A_2^*$), respectively; $A_1^* \simeq 83$ and $A_2^* \simeq 1287$. Examples are given for various values of A ; 1st stage ($A = 10$), 2nd stage ($A = 150, 400$ and 800), and 3rd stage ($A = 2000, 5000$, and 10^4).

For further analysis of dynamical responses, we decompose the whole population of RS neurons into two sub-populations of the stimulated and the non-stimulated RS neurons. Dynamical responses in these two sub-populations are shown well in Fig. 3. Raster plots of spikes, instantaneous sub-population spike rate (ISPSR) kernel estimates $R_s^{(1)}(t)$ and $R_s^{(2)}(t)$ [the superscript 1 (2) corresponds to the stimulated (non-stimulated) case], and power spectra of $\Delta R_s^{(1)}(t)$ and $\Delta R_s^{(2)}(t)$ in the stimulated and the non-stimulated sub-populations are shown in Fig. 3a1–a8, b1–b8, and c1–c8, respectively: the upper (lower) panels in these figures represent those for the stimulated (non-stimulated) case. Hereafter, the band width of the Gaussian kernel estimate for each ISPSR $R_s^{(l)}(t)$ ($l = 1$ and 2) is 7 ms for the excitatory case and 0.5 ms for the inhibitory case. We also measure the degree of population synchronization in each of the stimulated and the non-stimulated sub-populations by employing a realistic statistical-mechanical spiking measure, which was developed in our recent work

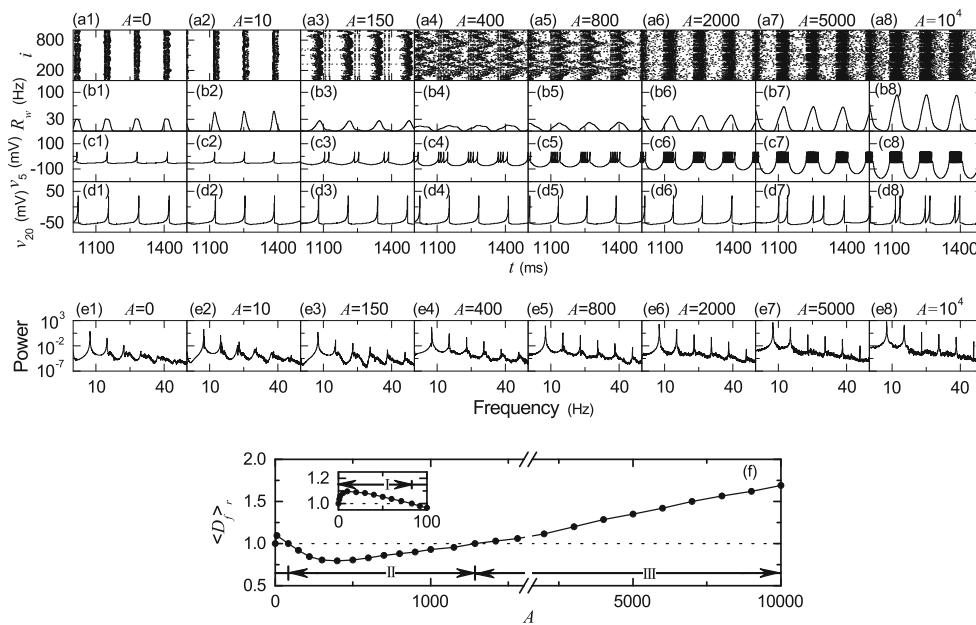


Fig. 2 Dynamical response when an external time-periodic stimulus $S(t)$ is applied to 50 randomly-chosen Izhikevich RS pyramidal neurons in the case of excitatory synchronization for $J = 15$ in Fig. 1. Raster plots of spikes, instantaneous whole-population spike rate (IWPSR) kernel estimates $R_w(t)$, membrane potentials $v_5(t)$ of the stimulated 5th RS pyramidal neuron, and membrane potentials $v_{20}(t)$ of the non-stimulated 20th RS pyramidal neuron are shown for various values of A in (a1)–(a8), (b1)–(b8), (c1)–(c8), and (d1)–(d8),

respectively. One-sided power spectra of $\Delta R_w(t) [= R_w(t) - \overline{R_w(t)}]$ (the overbar represents the time average) with mean-squared amplitude normalization are also given in (e1)–(e8). f Plot of dynamical response factor $\langle D_f \rangle_r$ versus A , where I, II, and III represent the 1st (synchronization enhancement), the 2nd (synchronization suppression), and the 3rd (synchronization enhancement) stages, respectively

(Kim and Lim 2014). As shown in Figs. 3a1–a8, population synchronization may be well visualized in a raster plot of spikes. For a synchronized case, the raster plot is composed of spiking stripes or bursting bands (indicating population synchronization). To measure the degree of the population synchronization seen in the raster plot, a statistical-mechanical spiking measure $M_s^{(l)}$ of Eq. (19), based on the IPSR kernel estimates $R_s^{(l)}(t)$ [$l = 1$ (2) corresponds to the stimulated (non-stimulated) case], was introduced by considering the occupation degrees $O_i^{(l)}$ of Eq. (15) (representing the density of stripes/bands) and the pacing degrees $P_i^{(l)}$ of Eq. (18) (denoting the smearing of stripes/bands) of the spikes in the stripes/bands (Kim and Lim 2014); for more details, refer to “Appendix”. The average occupation degree $\langle \langle O_i^{(l)} \rangle \rangle_r$, the average pacing degree $\langle \langle P_i^{(l)} \rangle \rangle_r$, and the average statistical-mechanical spiking measure $\langle \langle M_s^{(l)} \rangle \rangle_r$ are shown in Fig. 3d1–d3, respectively. Here, $\langle \cdot \rangle$ and $\langle \cdot \rangle_r$ represent the averages over global cycles and realizations, respectively; the number of realizations is 30 (60) for the non-stimulated (stimulated) case because the number N_s ($= 50$) of stimulated neurons is much less than that of non-stimulated neurons. Moreover, we obtain the cross-correlation

function $C_{12}(\tau)$ between $R_s^{(1)}(t)$ and $R_s^{(2)}(t)$ of the two sub-populations:

$$C_{12}(\tau) = \frac{\overline{\Delta R_s^{(1)}(t + \tau) \Delta R_s^{(2)}(t)}}{\sqrt{\overline{\Delta R_s^{(1)}(t)^2}} \sqrt{\overline{\Delta R_s^{(2)}(t)^2}}}, \quad (12)$$

where $\Delta R_s^{(1)}(t) = R_s^{(1)}(t) - \overline{R_s^{(1)}(t)}$, $\Delta R_s^{(2)}(t) = R_s^{(2)}(t) - \overline{R_s^{(2)}(t)}$, and the overline denotes the time average. Then, the cross-correlation measure M_c between the stimulated and the non-stimulated sub-populations is given by the value of $C_{12}(\tau)$ at the zero-time lag:

$$M_c = C_{12}(0), \quad (13)$$

which corresponds to the Pearson’s correlation coefficient for pairs of $[R_s^{(1)}(t), R_s^{(2)}(t)]$ (Press et al. 1992). The cross-correlation functions $\langle C_{12}(\tau) \rangle_r$ for various values of A are shown in Fig. 3e1–e8, f shows a plot of $\langle M_c \rangle_r$ versus A ; $\langle C_{12}(\tau) \rangle_r$ and $\langle M_c \rangle_r$ are obtained via an average over 30 realizations. Hereafter, the number of data used for the calculation of each temporal cross-correlation function $C_{12}(\tau)$ is $2^{16} (= 65536)$ in each realization.

We consider the 1st stage [$0 < A < A_1^* (\simeq 83)$] where synchronization enhancement with $\langle D_f \rangle_r > 1$ occurs. For

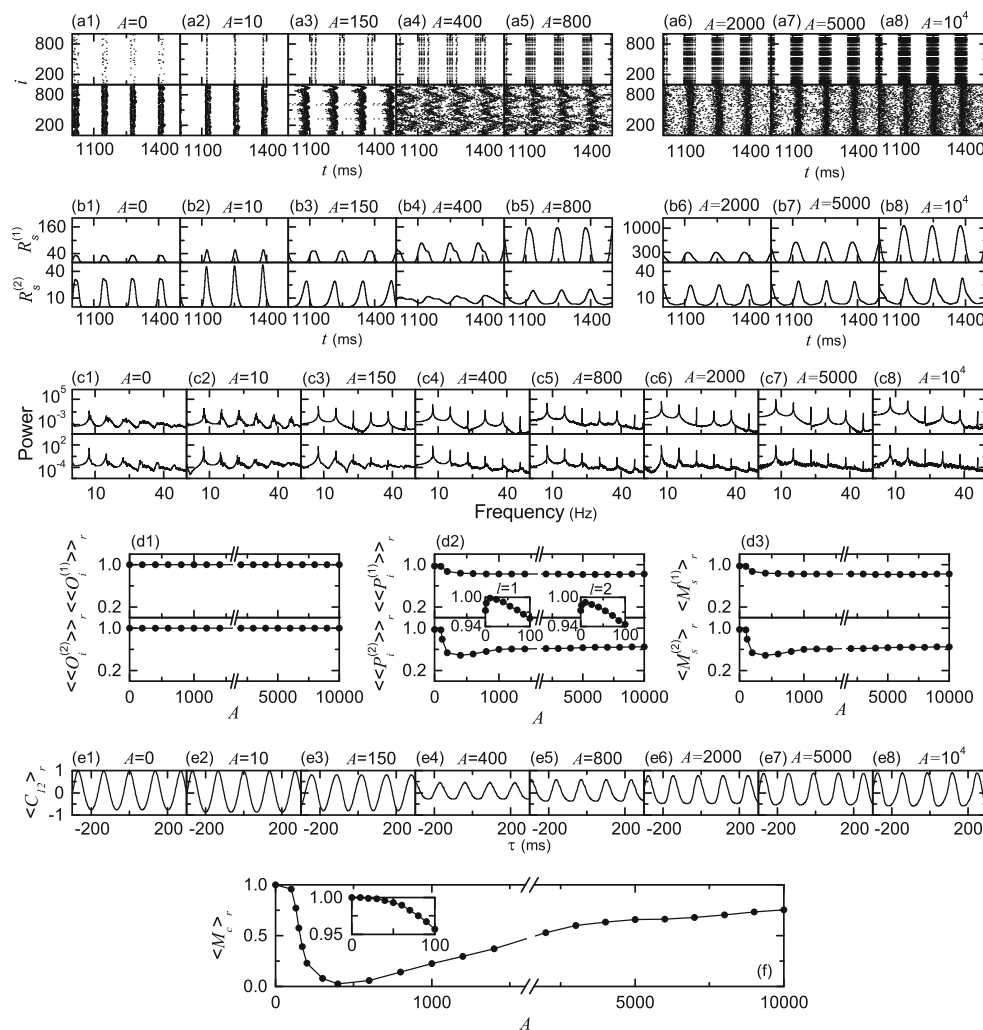


Fig. 3 Dynamical responses for the case of Fig. 2 in both the stimulated and the non-stimulated sub-populations and a cross-correlation measure $\langle M_c \rangle_r$ between the dynamics of the two sub-populations. Raster plot of spikes, instantaneous sub-population spike rates (ISPSRs) $R_s^{(1)}$ and $R_s^{(2)}$ [the superscript 1 (2) corresponds to the stimulated (non-stimulated) case], and one-sided power spectra of $\Delta R_s^{(1)}(t) [= R_s^{(1)}(t) - \overline{R_s^{(1)}}]$ and $\Delta R_s^{(2)}(t) [= R_s^{(2)}(t) - \overline{R_s^{(2)}}]$ (the overbar represents the time average) with mean-squared amplitude normalization in the stimulated and the non-stimulated sub-

populations are shown for various values of A in (a1)–(a8), (b1)–(b8), and (c1)–(c8), respectively: the upper (lower) panels denote those for the stimulated (non-stimulated) case. Plots of the average occupation degree $\langle \langle O_i^{(l)} \rangle \rangle_r$, the average pacing degree $\langle \langle P_i^{(l)} \rangle \rangle_r$, and the statistical-mechanical spiking measure $\langle M_s^{(l)} \rangle_r$ versus A are shown in (d1)–(d3), respectively; $l = 1$ (2) corresponds to the stimulated (non-stimulated) case. Plots of cross-correlation functions $\langle C_{12}(\tau) \rangle_r$ versus τ are also given in (e1)–(e8). f Plot of the cross-correlation measure $\langle M_c \rangle_r$ versus A

small A , stimulated RS neurons exhibit spikings which are phase-locked to external AC stimulus $S(t)$ [e.g., see Figs. 2c2 and 3a2 for $A = 10$]. [In Fig. 3, the upper (lower) panels correspond to the stimulated (non-stimulated) case.] Non-stimulated RS neurons also show spikings which are well matched with those of stimulated neurons thanks to phase-attractive effect of synaptic excitation, as shown in Figs. 2d2 and 3a2 for $A = 10$. For the case of $A = 10$, the widths of stripes in the raster plot of spikes are reduced in comparison with those for $A = 0$ [compare Fig. 2a2 with a1], which implies an increase in the degree of population synchronization. Hence, the oscillating amplitudes of

$R_w(t)$, $R_s^{(1)}(t)$, and $R_s^{(2)}(t)$ for $A = 10$ become larger than those for $A = 0$ [compare Figs. 2b2 and 3b2 with 2b1 and 3b1]. Peaks in the power spectra of $\Delta R_w(t)$, $\Delta R_s^{(1)}(t)$, and $\Delta R_s^{(2)}(t)$, associated with external phase-lockings of both stimulated and non-stimulated RS neurons, appear at the driving frequency f_d ($= 7.6$ Hz) and its harmonics, as shown in Figs. 2e2 and 3c2, respectively. In this way, synchronization enhancement occurs, and $\langle D_f \rangle_r$ increases until $A = 10$ [see the inset of Fig. 2f]. However, for $A > 10$ stimulated RS neurons begin to exhibit burstings, in contrast to spiking of non-stimulated RS neurons. Then, due to

difference in the type of firings of individual neurons, it is not easy for the spikings of non-stimulated RS neurons to be well matched with burstings of stimulated RS neurons. With increasing A , this type of mismatching begins to be gradually intensified, and the degree of population synchronization decreases. Hence, $\langle D_f \rangle_r$ begins to decrease for $A > 10$, as shown in the inset of Fig. 2f.

Eventually, when passing the 1st threshold $A_1^* (\simeq 83)$, a 2nd stage [$A_1^* < A < A_2^* (\simeq 1287)$] appears where synchronization suppression with $\langle D_f \rangle_r < 1$ occurs [see Fig. 2f]. For this case, stimulated RS neurons exhibit burstings which are phase-locked to external AC stimulus $S(t)$. As shown in Fig. 2c3–c5 for the membrane potential $v_5(t)$ of the 5th stimulated RS neuron in the stage II, with increasing A the number of spikes in each bursting increases. On the other hand, non-stimulated RS neurons show persistent spikings which are not well matched with burstings of stimulated neurons [e.g., see Fig. 2d3–d5 for the membrane potential $v_{20}(t)$ of the 20th non-stimulated RS neuron]. As an example, consider the case of $A = 150$. Stimulated RS neurons exhibit burstings, each of which consists of two spikes, as shown in Fig. 2c3. These burstings are synchronized, and hence a pair of vertical trains (composed of synchronized spikes in burstings) appear successively in the raster plot of spikes, as shown in the upper panel of Fig. 3a3. On the other hand, spiking stripes of non-stimulated RS neurons are smeared in a zigzag way between the synchronized vertical bursting trains (i.e., the pacing degree between spikes of non-stimulated RS neurons is reduced) [see the lower panel of Fig. 3a3]. This zigzag pattern (indicating local clustering of spikes) in the smeared stripes seems to appear because the Watts–Strogatz SWN with $p = 0.2$ has a relatively high clustering coefficient (denoting cliquishness of a typical neighborhood in the network) (Kim and Lim 2015b). These zigzag smeared stripes also appear in a nearly regular way with the driving frequency f_d , like the case of vertical bursting trains of stimulated RS neurons (see Fig. 3a3). Hence, both cases of stimulated and non-stimulated RS neurons are phase-locked to external AC stimulus, although they are mismatched (i.e., phase-shifted). Peaks of in power spectra $\Delta R_w(t)$, $\Delta R_s^{(1)}(t)$, and $\Delta R_s^{(2)}(t)$, corresponding to these external phase-lockings, appear at the driving frequency f_d and its harmonics, as shown in Figs. 2e3 and 3c3, respectively. Phase-shifted mixing of synchronized vertical bursting trains (of stimulated RS neurons) and zigzag smeared spiking stripes (of non-stimulated RS neurons) leads to decrease in the degree of population synchronization. Consequently, the amplitudes of $R_w(t)$ and $R_s^{(2)}(t)$ for $A = 150$ are smaller than those for $A = 10$ (compare Figs. 2b3 and 3b3 with 2b2 and 3b2), and synchronization suppression (with $\langle D_f \rangle_r < 1$) occurs (see Fig. 2f). As A is

further increased, more number of synchronized vertical bursting trains (phase-locked to external stimulus) appear successively in the raster plot of spikes, because each bursting of stimulated RS neurons consists of more number of spikes. Zigzag smearing of spiking stripes of non-stimulated RS neurons becomes intensified (i.e., the pacing degree between spikes of non-stimulated RS neurons becomes worse), although they are phase-locked to external AC stimulus. These bursting trains and smeared spiking stripes are still phase-shifted. In this way, with increasing A , the degree of population synchronization is decreased mainly due to smearing of spiking stripes, and eventually a minimum ($\simeq 0.7937$) of $\langle D_f \rangle_r$ occurs for $A = A_{min}^{(1)} (\simeq 398)$, as shown in Fig. 2f. An example near this minimum is given for the case of $A = 400$. A quadruple of vertical trains (consisting of synchronized spikes in burstings of stimulated RS neurons) and zigzag smeared spiking stripes of non-stimulated RS neurons appear successively in the raster plot of spikes, as shown in Fig. 3a4. Both of them are phase-locked to external stimulus, but they are more phase-shifted. Peaks of power spectra $\Delta R_w(t)$, $\Delta R_s^{(1)}(t)$, and $\Delta R_s^{(2)}(t)$, related to external phase-lockings for both cases of stimulated and non-stimulated RS neurons, also appear at the driving frequency f_d and its harmonics (see Figs. 2e4 and 3c4). Furthermore, the spiking stripes of non-stimulated RS neurons are much more smeared in a zigzag way when compared with the case of $A = 150$ (compare Fig. 3a4 with a3). Hence, the amplitudes of $R_w(t)$ and $R_s^{(2)}(t)$ become smaller than those for $A = 150$ (i.e., the degree of population synchronization is more reduced) (compare Figs. 2b4 and 3b4 with Figs. 2b3 and 3b3).

However, with further increase in A from $A_{min}^{(1)}$, synchronized burstings of stimulated RS neurons are more developed. Moreover, widths of zigzag smeared spiking stripes of non-stimulated RS neurons become gradually reduced [i.e., the degree of mismatching (phase-shift) between the stimulated and the non-stimulated sub-populations becomes decreased]. A constructive effect of $S(t)$ (resulting from a phase-attractive synaptic excitation) seems to appear effectively. Consequently, the degree of population synchronization begins to increase (i.e., $\langle D_f \rangle_r$ starts to grow). As an example, we consider the case of $A = 800$. Both the bursting bands (composed of spikes in burstings of the stimulated RS neurons) and the spiking stripes of non-stimulated RS neurons, phase-locked to external AC stimulus, appear successively in the raster plots of spikes, as shown in Fig. 3a5. When compared with the case of $A = 400$, the bursting bands are more developed, and the degree of zigzag smearing of spiking stripes is reduced (compare Fig. 3a5 with 3a4). Both the bursting bands and the smeared stripes are phase-locked to external

AC stimulus, and their phase-shift is reduced. Peaks of power spectra $\Delta R_w(t)$, $\Delta R_s^{(1)}(t)$, and $\Delta R_s^{(2)}(t)$, related to external phase-lockings for both cases of stimulated and non-stimulated RS neurons, also appear at the driving frequency f_d and its harmonics (see Figs. 2e5 and 3c5). Hence, the amplitudes of $R_s^{(1)}(t)$ and $R_s^{(2)}(t)$ become larger than those for $A = 400$ (compare Fig. 3b5 with b4), which results in the increase in the amplitude of $R_w(t)$ (compare Fig. 2b5 with b4). As a result, the degree of population synchronization is larger than that for $A = 400$. In this way, with increasing A from $A_{min}^{(1)}$ the dynamical factor $\langle D_f \rangle_r$ is increased. Eventually, when passing the 2nd threshold $A_2^* (\simeq 1287)$, $\langle D_f \rangle_r$ passes the unity, and a 3rd stage appears, where synchronization enhancement with $\langle D_f \rangle_r > 1$ reappears thanks to a phase-attractive effect of synaptic excitation (see Fig. 2f). As examples, we consider the cases of $A = 2000, 5000$, and 10^4 . As A is increased in this 3rd stage, burstings of RS neurons are more developed (e.g., see Fig. 2c6–c8), and non-stimulated RS neurons also begin to fire burstings for sufficiently large A (e.g., see Fig. 2d7–d8). Then, synchronized bursting bands of stimulated RS neurons are more and more intensified, as shown in Fig. 3a6–a8. Moreover, “firing” bands, composed of spikings/burstings of non-stimulated RS neurons, become matched well with bursting bands of stimulated RS neurons (see Fig. 3a6–a8): the matching degree also increases with A . Peaks of power spectra $\Delta R_w(t)$, $\Delta R_s^{(1)}(t)$, and $\Delta R_s^{(2)}(t)$, related to external phase-lockings for both cases of stimulated and non-stimulated RS neurons, appear at the driving frequency f_d and its harmonics (see Figs. 2e6–e8 and 3c6–c8). Consequently, with increasing A the amplitudes of both $R_s^{(1)}(t)$ and $R_s^{(2)}(t)$ are increased, as shown in Fig. 3b6–b8, which also leads to increase in $R_w(t)$ (see Fig. 2b6–b8). In this way, $\langle D_f \rangle_r$ increases monotonically with A and synchronization enhancement occurs in the 3rd stage, as shown in Fig. 2f.

By varying A , we also characterize population synchronization in each of the stimulated and the non-stimulated sub-populations in terms of the average occupation degree $\langle \langle O_i^{(l)} \rangle \rangle_r$, the average pacing degree $\langle \langle P_i^{(l)} \rangle \rangle_r$, and the average statistical-mechanical spiking measure $\langle M_s^{(l)} \rangle_r$; $l = 1$ and 2 correspond to the stimulated and the non-stimulated cases, respectively. Plots of $\langle \langle O_i^{(l)} \rangle \rangle_r$, $\langle \langle P_i^{(l)} \rangle \rangle_r$, and $\langle M_s^{(l)} \rangle_r$ versus A are shown in Fig. 3d1–d3, respectively. As A is increased, external phase lockings of spikings or burstings of stimulated RS neurons are more and more enhanced, as shown in Fig. 3a1–a8. Hence, the stimulated RS neurons exhibit full synchronization with $\langle \langle O_i^{(1)} \rangle \rangle_r = 1$, independently of A because every stimulated RS neuron makes a firing in each spiking stripe or bursting

band [corresponding to each global cycle of $R_s^{(1)}(t)$]. These fully synchronized spikes also show high average pacing degree $\langle \langle P_i^{(1)} \rangle \rangle_r$. For $0 < A < 10$, $\langle \langle P_i^{(1)} \rangle \rangle_r$ increases monotonically from 0.973 to 0.997 because smearing of spiking stripes (i.e. width of spiking stripes) becomes reduced (see the left inset of Fig. 3d2). For $A > 10$ bursting bands appear, at first their widths increase, but eventually they become saturated for large A (see Fig. 3a3–a8). Hence, for $A > 10$ $\langle \langle P_i^{(1)} \rangle \rangle_r$ begins to decrease, but it seems to approach a limit value ($\simeq 0.82$). Consequently, the average statistical-mechanical spiking measure $\langle M_s^{(1)} \rangle_r$ (given by taking into consideration both the occupation and the pacing degrees) exhibit the same behaviors with A as $\langle \langle P_i^{(1)} \rangle \rangle_r$ because $\langle \langle O_i^{(1)} \rangle \rangle_r = 1$. We next consider the non-stimulated case. Non-stimulated RS neurons also exhibit full synchronization with $\langle \langle O_i^{(2)} \rangle \rangle_r = 1$, independently of A . However, the average pacing degree $\langle \langle P_i^{(2)} \rangle \rangle_r$ varies with A , differently from the stimulated case. For $0 < A < 10$, spikings of non-stimulated RS neurons are well matched with those of stimulated RS neurons thanks to phase-attractive effect of synaptic excitation, and hence the average pacing degree $\langle \langle P_i^{(2)} \rangle \rangle_r$ increases monotonically from 0.973 to 0.989 (see the right inset of Fig. 3d2). However, for $A > 10$ it is not easy for spikings of non-stimulated neurons to be well matched with burstings of stimulated neurons because of different firing type. Hence, zigzag smearing occurs in the spiking stripes of non-stimulated neurons, and it is enhanced with A . Due to such developed zigzag smearing, $\langle \langle P_i^{(2)} \rangle \rangle_r$ decreases with A , and it arrives at its minimum ($\simeq 0.483$) for $A \simeq 391$. As A is further increased from the minimum point, zigzag smearing begins to be gradually reduced thanks to a constructive effect of $S(t)$ (coming from the phase-attractive synaptic excitation). As a result, $\langle \langle P_i^{(2)} \rangle \rangle_r$ starts to increase, and its value becomes large for large A (e.g., $\langle \langle P_i^{(2)} \rangle \rangle_r \simeq 0.65$ for $A = 10^4$). The average statistical-mechanical spiking measure $\langle M_s^{(2)} \rangle_r$ also show the same behaviors with A as $\langle \langle P_i^{(2)} \rangle \rangle_r$ because $\langle \langle O_i^{(2)} \rangle \rangle_r = 1$.

Finally, to examine the matching degree between the stimulated and the non-stimulated sub-populations, we obtain the cross-correlation functions $\langle C_{12}(\tau) \rangle_r$ between $R_s^{(1)}(t)$ and $R_s^{(2)}(t)$ of the two sub-populations, which are shown for various values of A in Fig. 3e1–e8. A plot of the cross-correlation measure $\langle M_c \rangle_r$ [given by $C_{12}(0)$] versus A is also shown in Fig. 3f. Perfect cross-correlation with $\langle M_c \rangle_r = 1$ occurs in the range of $0 < A < 10$ where $\langle D_f \rangle_r$ increases monotonically from 1 to its maximum ($\simeq 1.095$) at $A = 10$ (see the inset in Fig. 2f). In the remaining region ($10 < A < A_1^*$) of the 1st stage, $\langle M_c \rangle_r$

decreases slowly, but it still indicates strong cross-correlation with $\langle M_c \rangle_r > 0.97$. This type of perfect/strong cross-correlation induces phase-attractive effect between the stimulated and the non-stimulated sub-populations, and hence synchronization enhancement occurs in the stage I. However, in the first part of the 2nd stage $\langle M_c \rangle_r$ decreases very rapidly to its minimum for $A \simeq 403$ (which is nearly the same as $A_{min}^{(1)} (\simeq 398)$ for the minimum of $\langle D_f \rangle_r$), mainly because of the different firing type of the stimulated RS neurons (bursting) and the non-stimulated RS neurons (spiking). Due to sudden decrease in the cross-correlation, $\langle D_f \rangle_r$ also decreases from 1, and synchronization suppression occurs. After passing the minimum point ($A \simeq 403$), $\langle M_c \rangle_r$ begins to increase gradually with A , thanks to a phase-attractive effect of the excitatory coupling. Consequently, in the latter part of the 2nd stage (with $\langle D_f \rangle_r < 1$) $\langle D_f \rangle_r$ increases monotonically with A , and eventually when passing the 2nd threshold $A_2^* (\simeq 1287)$ $\langle D_f \rangle_r$ passes the unity. Thus, the 3rd stage appears, and synchronization enhancement reoccurs.

Dynamical responses of inhibitory synchronization to an external time-periodic stimulus

We consider an inhibitory Watts–Strogatz SWN composed of $N (= 10^3)$ Izhikevich FS interneurons. Figure 4a shows a plot of the firing frequency f versus the external DC current I_{DC} for a single Izhikevich FS interneuron in the absence of noise ($D = 0$). The Izhikevich FS interneuron exhibits a jump from a resting state to a spiking state via subcritical Hopf bifurcation at a higher threshold $I_{DC,h} (\simeq 73.7)$ by absorbing an unstable limit cycle born through a fold limit cycle bifurcation for a lower threshold $I_{DC,l} (\simeq 72.8)$. Hence, the Izhikevich FS interneuron exhibits type-II excitability because it begins to fire with a non-zero frequency (Izhikevich 2007; Hodgkin 1948; Izhikevich 2000). As I_{DC} is increased from $I_{DC,h}$, the firing frequency f increases monotonically. Here, we consider a suprathreshold case of $I_{DC} = 1500$ in the presence of noise with $D = 50$ for which a time series of the membrane potential v with an oscillating frequency $f \simeq 635$ Hz is shown in Fig. 4b. As an example, we consider a coupling case of $J = 100$. Full synchronization for $J = 100$ is well shown in the raster plot of spikes in Fig. 4c1. For this case, the IWPSR kernel estimate $R_w(t)$ exhibits a regular oscillation with a fast population frequency $f_p (\simeq 200$ Hz) (see the peak in the power spectrum of $\Delta R_w(t)$ in Fig. 4d). The ISI histogram for individual interneurons is also shown in Fig. 4e. The ensemble-averaged ISI $\langle ISI \rangle$ is 5.0 ms, and hence the ensemble-averaged MFR $\langle f_i \rangle$ of individual interneurons (corresponding to the reciprocal of $\langle ISI \rangle$) is 200 Hz, which is the same as f_p .

We apply an external time-periodic AC stimulus $S(t)$ to $N_s (= 50)$ randomly-selected Izhikevich FS interneurons by fixing the driving angular frequency as $\omega_d (= 2\pi f_d) = 1.26$ rad/ms ($f_d = \langle f_i \rangle = 200$ Hz), and investigate the dynamical response of inhibitory full synchronization by varying the driving amplitude A . Figure 5a1–a8 show raster plots of spikes for various values of A . Population synchronization may be well seen in these raster plots of spikes. The IWPSR kernel estimates $R_w(t)$, exhibiting oscillatory behaviors, are shown in Fig. 5b1–b8, and the power spectra of $\Delta R_w(t)$ are also given in Fig. 5f1–f8. In addition, times series of membrane potentials of individual FS interneurons are given for various values of A . The time series of $v_5(t)$ of the 5th stimulated FS interneuron are shown in Fig. 5c1–c8. For the non-stimulated case, there are two types of FS interneurons, depending on their synaptic connections. Many non-stimulated FS interneurons (i.e., major non-stimulated FS interneurons) which have synaptic connections with fast-firing stimulated FS interneurons fire slowly due to increased inhibition. On the other hand, a small number of non-stimulated FS interneurons (i.e., minor non-stimulated FS interneurons) which have no direct synaptic connections with stimulated FS interneurons receive synaptic inputs from major slowly-firing non-stimulated FS interneurons, and hence MFRs of minor non-stimulated FS interneurons become fast due to decreased inhibition. Figure 5d1–d8 show the time series of $v_{20}(t)$ of the 20th major slowly-firing non-stimulated FS interneuron, while Fig. 5e1–e8 show the time series of $v_{115}(t)$ of the 115th minor fast-firing non-stimulated FS interneuron. A plot of the dynamical factor $\langle D_f \rangle_r$ versus A is given in Fig. 5g. Two stages are thus found to appear. Synchronization suppression ($\langle D_f \rangle_r < 1$) and synchronization enhancement ($\langle D_f \rangle_r > 1$) occur in the 1st (I) stage ($0 < A < A_3^*$) and the 2nd (II) stage ($A > A_3^*$), respectively, where $A_3^* \simeq 49699$. Examples are given for various values of A ; 1st stage ($A = 1000, 3000, 5000, 8000, 10^4$, and 3×10^4) and 2nd stage ($A = 6 \times 10^4$).

As in the above excitatory case, we make more detailed analysis of dynamical responses by decomposing the whole population of FS interneurons into two sub-populations of the stimulated and the non-stimulated FS interneurons. Dynamical responses in these two sub-populations are shown well in Fig. 6. Raster plots of spikes, ISPSR kernel estimates $R_s^{(1)}(t)$ and $R_s^{(2)}(t)$ [the superscript 1 (2) corresponds to the stimulated (non-stimulated) case], and power spectra of $\Delta R_s^{(1)}(t)$ and $\Delta R_s^{(2)}(t)$ in the stimulated and the non-stimulated sub-populations are shown in Fig. 6a1–a8, b1–b8, and c1–c8, respectively: the upper (lower) panels in these figures represent those for the stimulated (non-stimulated) case. For characterization of population synchronization in each of the stimulated and the non-stimulated

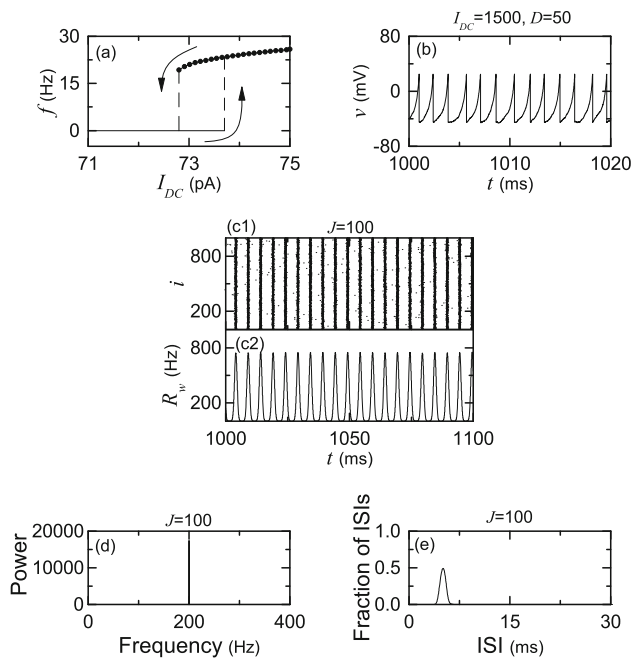


Fig. 4 Inhibitory synchronization in the Watts–Strogatz SWN of $N(=10^3)$ Izhikevich FS interneurons for $M_{syn} = 50$ and $p = 0.2$. Single Izhikevich FS interneuron: **a** plot of the mean firing rate f versus the external DC current I_{DC} for $D = 0$ and **b** time series of the membrane potential v for $I_{DC} = 1500$ and $D = 50$. Coupled Izhikevich FS interneurons for $I_{DC} = 1500$, $D = 50$, and $J = 100$: **c1** raster plot of spikes, **c2** plot of the instantaneous whole-population spike rate (IWPSR) kernel estimate $R_w(t)$ versus t , **d** one-sided power spectrum of $\Delta R_s(t) [= R_w(t) - \overline{R_w(t)}]$ (the overbar represents the time average) with mean-squared amplitude normalization, and **e** inter-spike interval (ISI) histogram

sub-populations, the average occupation degree $\langle \langle O_i^{(l)} \rangle \rangle_r$, the average pacing degree $\langle \langle P_i^{(l)} \rangle \rangle_r$, and the average statistical-mechanical spiking measure $\langle M_s^{(l)} \rangle_r$ are given in Fig. 6d1–d3, respectively; $l = 1$ (2) represents the stimulated (non-stimulated) case. The cross-correlation functions $\langle C_{12}(\tau) \rangle_r$ between $R_s^{(1)}(t)$ and $R_s^{(2)}(t)$ of the two sub-populations are also shown for various values of A in Fig. 6e1–e8. Figure 6f shows a plot of the cross-correlation measure $\langle M_c \rangle_r$ [given by $C_{12}(0)$] versus A .

As A is increased from 0 and passes a threshold, stimulated FS interneurons begin to exhibit burstings, as shown in Fig. 5c2–c8, and the number of spikings in each bursting increases with A . These burstings are phase-locked to external stimulus $S(t)$, which are intensified with increasing A (see the upper panels of Fig. 6a2–a8). Consequently, as A is increased, the amplitude of $R_s^{(1)}(t)$ also increases, as shown in Fig. 6b2–b8. Peaks in the power spectrum of $\Delta R_s^{(1)}(t)$, associated with the external phase lockings, appear at the driving frequency $f_d (= 200 \text{ Hz})$ and its harmonics (see the upper panels of Fig. 6c2–c8). This kind of

external phase lockings of stimulated FS interneurons are similar to those for the case of excitatory coupling. However, the external stimulus $S(t)$ makes a destructive effect on the sub-population of non-stimulated FS interneurons, in contrast to the excitatory case (where a constructive effect of $S(t)$, resulting from the phase-attractive synaptic excitation, leads to external phase lockings of non-stimulated RS neurons).

In the presence of burstings of stimulated FS interneurons, spikings of non-stimulated FS interneurons cannot be well matched with burstings of stimulated FS interneurons, because of difference in the type of firings of individual neurons (e.g., see Fig. 6a2 for $A = 1000$). However, these spiking stripes of non-stimulated FS interneurons are also phase-locked to external stimulus, although they are phase-shifted from the vertical bursting trains of the stimulated FS interneurons. Peaks in the power spectrum of $\Delta R_s^{(2)}(t)$, related to the external phase lockings, appear at the driving frequency $f_d (= 200 \text{ Hz})$ and its harmonics (see the lower panel of Fig. 6c2). As A is further increased, a destructive effect of $S(t)$, resulting from repulsive synaptic inhibition, becomes intensified. Hence, zigzag smearing pattern appears in their spiking stripes, as shown in Fig. 6a3 for $A = 3000$. As explained in the excitatory case, such zigzag pattern in the smeared stripes seems to appear because the Watts–Strogatz SWN with $p = 0.2$ has a relatively high clustering coefficient (Kim and Lim 2015b). Furthermore, major non-stimulated FS interneurons begin to exhibit intermittent and stochastic spikings (i.e., stochastic spike skipping) (Golomb and Rinzel 1994; Longtin 1995, 2000). Due to the stochastic spike skipping, the original full synchronization (where all the non-stimulated FS interneurons fire spikings in each spiking stripe) in the non-stimulated sub-population begins to break up, and a sparse synchronization (where only some fraction of non-stimulated FS interneurons fire spikings in each spiking stripe) starts to appear (i.e., sparse spiking stripes begin to appear) (Brunel and Hakim 2008; Kim and Lim 2015b). (However, the degree of sparseness for $A = 3000$ is relatively low, and hence no skipings are found in $v_{20}(t)$ of the 20th major non-stimulated FS interneuron for a short time interval of 20 ms in Fig. 5d3). In this way, with increasing A the mismatching degree between the stimulated and the non-stimulated sub-populations is increased, although both the bursting bands of stimulated FS interneurons and the zigzag smeared sparse spiking stripes of non-stimulated FS interneurons are phase locked to external stimulus. Due to increased zigzag smearing, peaks at the driving frequency f_d and its harmonics for $A = 3000$ become more broad than those for $A = 1000$ (compare Fig. 6c3 with c2). The effect of zigzag smearing and stochastic spike skipping in the non-stimulated sub-population is more dominant when

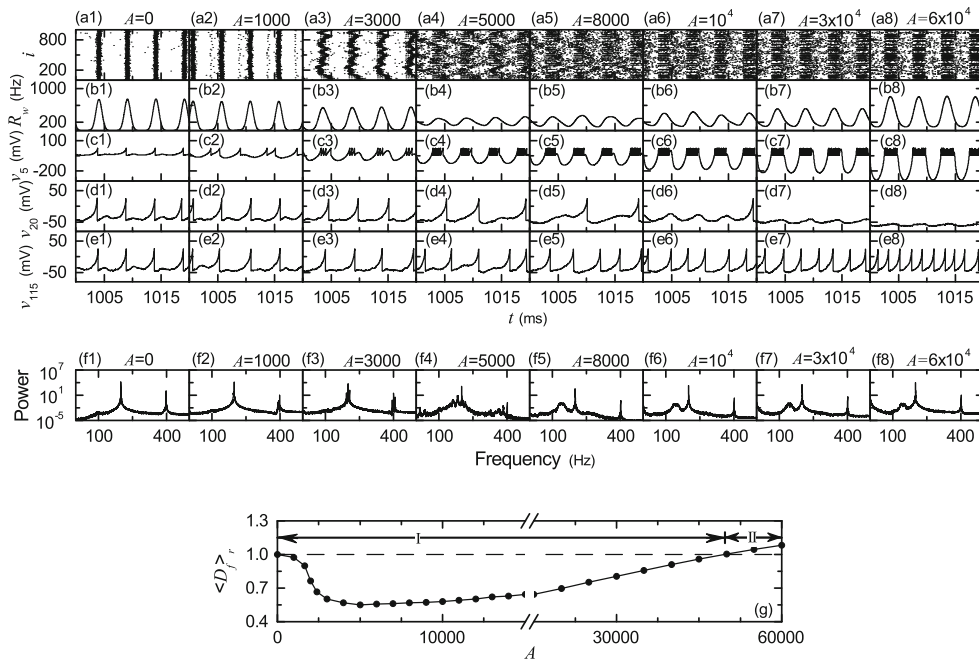


Fig. 5 Dynamical response when an external time-periodic stimulus $S(t)$ is applied to 50 randomly-chosen Izhikevich FS interneurons in the case of inhibitory synchronization for $J = 100$. Raster plots of spikes, instantaneous whole-population spike rate (IWPSR) kernel estimates $R_w(t)$, membrane potentials $v_5(t)$ of the stimulated 5th FS interneuron, membrane potentials $v_{20}(t)$ of the major non-stimulated 20th FS interneuron, and membrane potentials $v_{115}(t)$ of the minor non-stimulated 115th FS interneuron are shown for various values of

A in (a1)–(a8), (b1)–(b8), (c1)–(c8), (d1)–(d8), and (e1)–(e8), respectively. One-sided power spectra of $\Delta R_w(t) [= R_w(t) - \overline{R_w(t)}]$ (the overbar represents the time average) with mean-squared amplitude normalization are also given in (f1)–(f8). **g** Plot of dynamical response factor $\langle D \rangle_r$ versus A , where I and II represent the 1st (synchronization suppression) and the 2nd (synchronization enhancement) stages, respectively

compared with the enhanced external phase lockings in the stimulated sub-population. Hence, the overall degree of population synchronization in the whole population becomes worse. As a result, for the case of $A = 3000$, the amplitudes of $R_s^{(2)}(t)$ and $R_w(t)$ are smaller than those for $A = 1000$ (see Figs. 6b3 and 5b3), and D_f decreases rapidly, as shown in Fig. 5g. With further increase in A , this tendency of zigzag smearing and stochastic spike skipping in the non-stimulated sub-population is intensified, and eventually D_f arrives at its minimum ($\simeq 0.548$) for $A = A_{min}^{(2)} (\simeq 4876)$. As an example near this minimum, we consider the case of $A = 5000$. For this case, stochastic spike skipping is more intensified (see Fig. 5d4), and hence the original full synchronization in the non-stimulated sub-population becomes broken up (i.e., sparse stripes in the raster plot of spikes appear). Particularly, such sparse spiking stripes of non-stimulated FS interneurons are smeared in a zigzag way much more than those for the case of $A = 3000$ (compare Fig. 6a4 with a3). Consequently, the amplitudes of $R_s^{(2)}(t)$ and $R_w(t)$ are much smaller than those for $A = 3000$ (see Figs. 6b4 and 5b4) (i.e., the degree of population synchronization is reduced more significantly when compared with that for $A = 3000$). As shown in the lower panel of Fig. 6c4, peaks at the driving frequency f_d

and its harmonics also begin to be “disrupted” [i.e., their heights become smaller, and near f_d new tiny peaks (of frequencies 164 and 183 Hz) appear].

However, with further increase in A from $A_{min}^{(2)}$, non-stimulated FS interneurons begin to reorganize their spikings and exhibit a new type of sparse synchronization with the sub-population frequency $f_{sp}^{(2)} (\simeq 143 \text{ Hz})$, along with enhanced external phase lockings of burstings of stimulated FS interneurons with the sub-population frequency $f_{sp}^{(1)} (\simeq 200 \text{ Hz})$ (e.g., see the raster plots of spikes in Fig. 6a5, the ISPSR kernel estimates $R_s^{(1)}(t)$ and $R_s^{(2)}(t)$ in Fig. 6b5), and the power spectra in Fig. 6c5 for $A = 8000$]. A new peak, associated with sparse synchronization of non-stimulated FS interneurons, appears at $f \simeq 143 \text{ Hz}$, as shown in the lower panel of Fig. 6c5. [For $A = 8000$, the peak at the driving frequency f_d also coexists, but eventually it disappears for larger A (see Figs. 6c6–c8)]. This “sparse-synchronization” peak of 143 Hz comes from evolution of the (above) tiny peak of 164 Hz for $A = 5000$. With increasing A the frequency of the tiny peak at 164 Hz for $A = 5000$ becomes smaller, and for $A = 8000$ the peak becomes broad and its frequency becomes 143 Hz (On the other hand, as A is increased the height of another peak of 183 Hz for $A = 5000$ becomes smaller and it disappears).

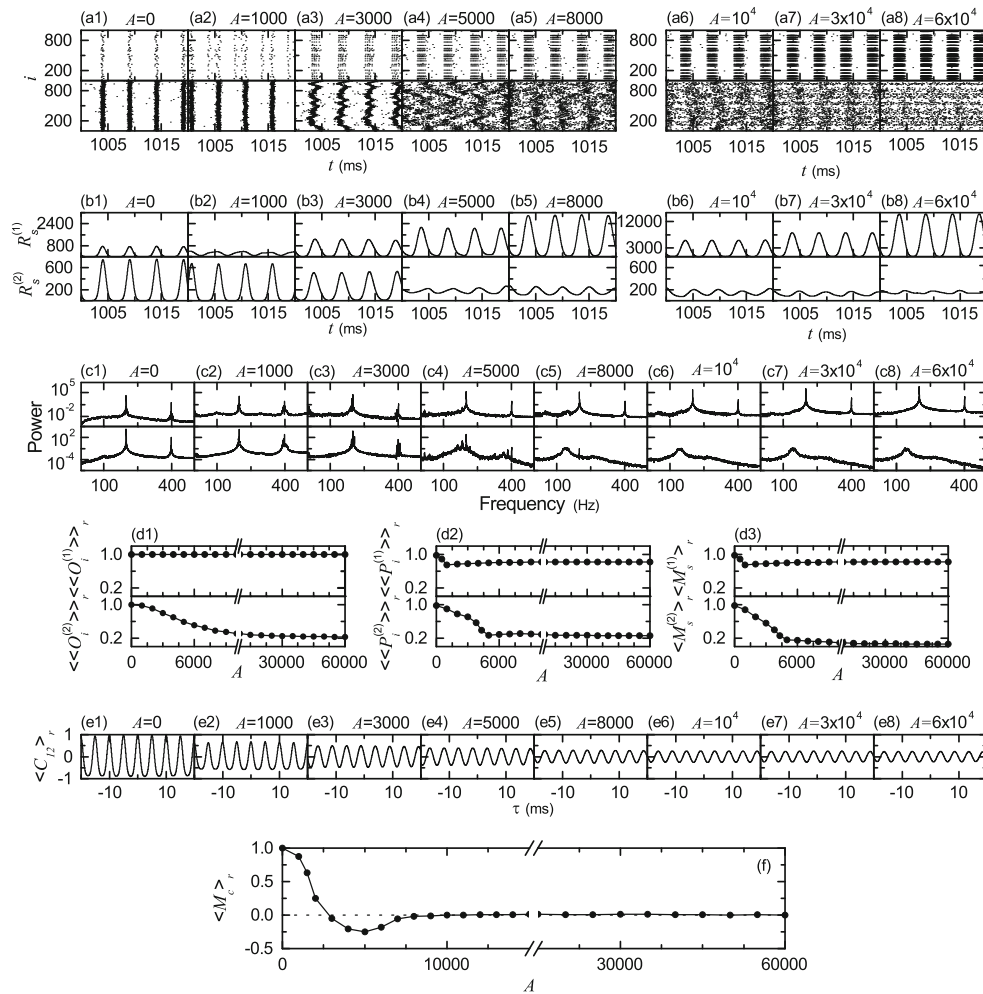


Fig. 6 Dynamical responses for the case of Fig. 5 in both the stimulated and the non-stimulated sub-populations and a cross-correlation measure $\langle M_c \rangle_r$ between the dynamics of the two sub-populations. Raster plot of spikes, instantaneous sub-population spike rates (ISPSRs) $R_s^{(1)}$ and $R_s^{(2)}$ [the superscript 1 (2) corresponds to the stimulated (non-stimulated) case], and one-sided power spectra of $\Delta R_s^{(1)}(t) [= R_s^{(1)}(t) - \overline{R_s^{(1)}}]$ and $\Delta R_s^{(2)}(t) [= R_s^{(2)}(t) - \overline{R_s^{(2)}}]$ (the overbar represents the time average) with mean-squared amplitude normalization in the stimulated and the non-stimulated sub-

populations are shown for various values of A in (a1)–(a8), (b1)–(b8), and (c1)–(c8), respectively: the upper (lower) panels denote those for the stimulated (non-stimulated) case. Plots of the average occupation degree $\langle \langle O_i^{(l)} \rangle \rangle_r$, the average pacing degree $\langle \langle P_i^{(l)} \rangle \rangle_r$, and the statistical-mechanical spiking measure $\langle \langle M_s^{(l)} \rangle \rangle_r$ versus A are shown in (d1)–(d3), respectively; $l = 1$ (2) corresponds to the stimulated (non-stimulated) case. Plots of cross-correlation functions $\langle C_{12}(\tau) \rangle_r$ versus τ are also given in (e1)–(e8). f Plot of the cross-correlation measure $\langle M_c \rangle_r$ versus A

Thanks to increase in the degree of synchronization in both the stimulated and the non-stimulated sub-populations, the amplitudes of both $R_s^{(1)}(t)$ and $R_s^{(2)}(t)$ become larger than those for $A = 5000$ (compare Fig. 6b5 with b4), which leads to the increase of the amplitude of $R_w(t)$ (see Fig. 5b5). As a result, D_f is increased, as shown in Fig. 5g. As A is further increased, external phase lockings of burstings with $f_{sp}^{(1)} \simeq 200$ Hz in the stimulated sub-population are more and more enhanced due to increased stimulation, while the degree of sparse synchronization with sub-population frequency $f_{sp}^{(2)}$ in the non-stimulated sub-population becomes worse due to stochastic spike skipping of major non-stimulated FS interneurons and

smearing of sparse stripes, as shown in the raster plots, the ISPSR kernel estimates $R_s^{(1)}(t)$ and $R_s^{(2)}(t)$, and the power spectra for $A = 10^4$, 3×10^4 , and 6×10^4 (see Fig. 6a6–a8, b6–b8, and c6–c8); $f_{sp}^{(2)} \simeq 145$, 146, and 146 Hz for $A = 10^4$, 3×10^4 , and 6×10^4 , respectively. Thanks to the dominance of external phase lockings in the stimulated sub-population, the overall degree of population synchronization in the whole population becomes better (i.e., the amplitudes of $R_w(t)$ increase, as shown in Figs. 5b6–b8), and hence D_f increases monotonically with A . Eventually when passing a threshold of $A_3^* (\simeq 49699)$, D_f becomes larger than 1, and then the 2nd stage appears where synchronization enhancement occurs, as shown in Fig. 5g.

We also characterize the population synchronization in each of the stimulated and the non-stimulated sub-populations by employing the average occupation degree $\langle\langle O_i^{(l)} \rangle\rangle_r$, the average pacing degree $\langle\langle P_i^{(l)} \rangle\rangle_r$, and the average statistical-mechanical spiking measure $\langle M_s^{(l)} \rangle_r$; $l = 1$ (2) represents the stimulated (non-stimulated) case. Plots of $\langle\langle O_i^{(l)} \rangle\rangle_r$, $\langle\langle P_i^{(l)} \rangle\rangle_r$, and $\langle M_s^{(l)} \rangle_r$ versus A are given in Fig. 6d1–d3, respectively. The average occupation degree $\langle\langle O_i^{(1)} \rangle\rangle_r$ is 1 (i.e., full synchronization occurs), independently of A , because every stimulated FS interneuron fires in each spiking stripe or bursting band. This inhibitory full synchronization in the stimulated sub-population also exhibits high pacing degree $\langle\langle P_i^{(1)} \rangle\rangle_r$, similar to the excitatory case. As A is increased from 0, $\langle\langle P_i^{(1)} \rangle\rangle_r$ begins to decrease, and arrives at a minimum ($\simeq 0.737$) for $A \simeq 1320$. Near the minimum point, stimulated interneurons show mixed burstings and spikings, as shown in Fig. 5a2 for $A = 1000$ where each bursting consists of two spikes whose separation is wide. However, with further increase in A external phase lockings of burstings of stimulated FS interneurons are more and more developed (see the developed bursting bands in Fig. 6a3–a8). Consequently, $\langle\langle P_i^{(1)} \rangle\rangle_r$ begins to increase, and it approaches a limit value ($\simeq 0.82$). For this type of full synchronization (i.e., $\langle\langle O_i^{(1)} \rangle\rangle_r = 1$), the average statistical-mechanical spiking measure $\langle M_s^{(1)} \rangle_r$ is the same as $\langle\langle P_i^{(1)} \rangle\rangle_r$. Unlike the stimulated case, when passing a threshold ($A \simeq 55$) (major) non-stimulated FS interneurons begin to exhibit stochastic spike skipping (i.e., intermittent and irregular spikings) due to a destructive effect of $S(t)$ (resulting from strong synaptic inhibition). Hence, $\langle\langle O_i^{(2)} \rangle\rangle_r$ varies depending on A in the non-stimulated sub-population. Below the threshold $\langle\langle O_i^{(2)} \rangle\rangle_r = 1$ (i.e., full synchronization takes place). However, above the threshold, sparse synchronization with $\langle\langle O_i^{(2)} \rangle\rangle_r < 1$ occurs (i.e., sparse stripes appears in the raster plots of spikes. as shown in Fig. 6a2–a8). With increasing A from the threshold, $\langle\langle O_i^{(2)} \rangle\rangle_r$ decreases monotonically, and its value becomes very low ($\simeq 0.23$) for large A , as shown in the lower panel of Fig. 6d1, which is in contrast to the excitatory case of full synchronization (see the lower panel in Fig. 3d1). As A is increased from the threshold, zigzag smearing in the spiking stripes is more enhanced (see Fig. 6a3–a4). As a result, $\langle\langle P_i^{(2)} \rangle\rangle_r$ decreases rapidly, and it arrives at a minimum ($\simeq 0.265$) for $A \simeq 4981$, as shown in Fig. 6d2. With increase in A from the minimum point, such zigzag smearing begins to be reduced, and non-stimulated FS interneurons reorganize their spikings to exhibit a new type of sparse synchronization (compare Fig. 6a5 with a4).

Then, $\langle\langle P_i^{(2)} \rangle\rangle_r$ increases a little, as shown in Fig. 6d2. However, as A is further increased, sparse spiking stripes become more smeared (see Fig. 6a6–a8), and hence $\langle\langle P_i^{(2)} \rangle\rangle_r$ decreases again; $\langle\langle P_i^{(2)} \rangle\rangle_r \simeq 0.26$ for large A . For this case of sparse synchronization, the average statistical-mechanical spiking measure $\langle M_s^{(2)} \rangle_r$ is less than $\langle\langle P_i^{(2)} \rangle\rangle_r$ because $\langle\langle O_i^{(2)} \rangle\rangle_r < 1$, unlike the full synchronization in the excitatory case.

For examination of the matching degree between the stimulated and the non-stimulated sub-populations, we get the cross-correlation functions $\langle C_{12}(\tau) \rangle_r$ between $R_s^{(1)}(t)$ and $R_s^{(2)}(t)$ of the two sub-populations, which are shown for various values of A in Fig. 6e1–e8. A plot of the cross-correlation measure $\langle M_c \rangle_r$ of Eq. (13) versus A is also given in Fig. 6f. Unlike the excitatory case, as A is increased from 0 $\langle M_c \rangle_r$ decreases monotonically to its minimum ($\simeq -0.242$) for $A \simeq 4890$ (which is nearly the same as $A_{min}^{(2)} (\simeq 4876)$ for the minimum of $\langle D_f \rangle_r$) due to a destructive effect of external stimulus $S(t)$ (causing the zigzag smearing and the stochastic spike skipping in the non-stimulated sub-population). Because of monotonic decrease in $\langle M_c \rangle_r$, $\langle D_f \rangle_r$ also decreases from 1, and synchronization suppression occurs. After passing the minimum point ($A \simeq 4890$), $\langle M_c \rangle_r$ begins to increase slowly with A , but eventually it approaches 0 (without further increase), in contrast to the excitatory case (where $\langle M_c \rangle_r$ continue to increase monotonically without saturation) (compare Fig. 6f with 3f). We also note that the oscillating amplitudes of $\langle C_{12}(\tau) \rangle_r$ decrease with A , as shown in Fig. 6e5–e8, unlike the excitatory case where the oscillating amplitudes of $\langle C_{12}(\tau) \rangle_r$ increase with A (see Fig. 3e5–e8). This weak cross-correlation between the stimulated and the non-stimulated sub-populations occurs due to completely different types of population behaviors in the two sub-populations: non-stimulated FS interneurons exhibit a new type of sparse synchronization of low degree (without any external phase lockings), while stimulated FS interneurons show external phase lockings of burstings. Due to stronger stimulation effect, external phase lockings of stimulated FS interneurons are more and more intensified, and they become dominant. As a result, with increasing A the overall degree of population synchronization in the whole population becomes better. Hence, both the amplitude of $R_w(t)$ and $\langle D_f \rangle_r$ increase monotonically with A (without saturation) (see Fig. 5b5–b8 and g), in spite of weak cross-correlations between the two sub-populations. However, the increasing rate for $\langle D_f \rangle_r$ is much slower when compared with that for the excitatory case where the increase in $\langle D_f \rangle_r$ results from cooperation of the two sub-populations with strong cross-correlations.

Summary

Brain rhythms appear in health and diseases via neural synchronization. A neural system's response to external stimulus can provide useful information about its dynamical properties. Therefore, it is important to investigate how an external stimulus affects the neural synchronization. Synchronization enhancement or suppression may occur via control of population synchronization. In most previous theoretical and computational works on control of population synchronization, only excitatory-type couplings were considered. To see the dependence of dynamical responses to external stimuli on the synaptic-coupling type, we considered two types of excitatory and inhibitory full synchronization in the Watts–Strogatz SWN of excitatory RS pyramidal neurons and inhibitory FS interneurons, and investigated the effects of synaptic interactions on dynamical responses to external time-periodic stimuli $S(t)$ by varying the driving amplitude A . We have characterized dynamical responses to $S(t)$ in terms of the dynamical response factor $\langle D_f \rangle_r$ by increasing A . For the case of excitatory coupling, external phase lockings occur in both the stimulated and the non-stimulated sub-populations, thanks to a constructive effect of $S(t)$ which results from phase-attractive synaptic excitation. On the other hand, in the case of inhibitory coupling, external phase locking occurs only in the stimulated sub-population, while the original inhibitory full synchronization in the non-stimulated sub-population breaks up gradually (i.e., for large A non-stimulated FS interneurons exhibit a new type of inhibitory sparse synchronization of low degree) due to a destructive effect of $S(t)$ which comes from strong synaptic inhibition. As results of these different effects of $S(t)$, the type and degree of dynamical response (e.g., synchronization enhancement or suppression characterized by $\langle D_f \rangle_r$) have been found to vary differently, depending on the type of synaptic interaction. For a detailed analysis, we have also measured the matching degree between the dynamics of the two sub-populations of stimulated and non-stimulated neurons in terms of a cross-correlation measure $\langle M_c \rangle_r$. $\langle M_c \rangle_r$ has been found to vary with A in a different way, depending on the synaptic-coupling type. For small A , synchronization enhancement occurs for the excitatory case, thanks to strong cross-correlation (with $\langle M_c \rangle_r > 0.97$) between the two sub-populations, while synchronization suppression takes place in the inhibitory case, due to monotonic decrease in $\langle M_c \rangle_r$. Particularly, for large A the cross-correlation becomes very weak in the inhibitory case, while for the excitatory case $\langle M_c \rangle_r$ increases gradually after passing its minimum (i.e., it becomes large for large A). Consequently, in the

excitatory case synchronization enhancement reappears for an intermediate value of A , thanks to the strong cross-correlation: with increasing A from 0, synchronization enhancement first appears, then synchronization suppression occurs, and finally synchronization enhancement reappears. For the inhibitory case, in spite of weak cross-correlation, synchronization enhancement also appears for sufficiently large A , just thanks to much-enhanced external phase lockings of burstings of stimulated FS interneurons: with increase in A from 0, synchronization suppression appears in a wide range of A , and then synchronization enhancement occurs for very large A . However, occurrence of synchronization enhancement for the inhibitory case might be improbable because the threshold value for appearance of synchronization enhancement seems to be enormously large beyond the relevant physiological range. All these results for both excitatory and inhibitory cases are expected to provide useful insights on the dynamical responses to external stimuli in neural systems (i.e., how external stimuli affect brain rhythms emerging via excitatory and inhibitory synchronization).

In this work, we employed the Watts–Strogatz small-world network as a complex network. However, we think that our results would be largely valid, independently of network architecture, because dynamical responses to external time-periodic stimuli depend just on the synaptic-coupling type (excitatory or inhibitory). In addition to simple Izhikevich spiking neuron model we studied, investigations of dynamical responses to external stimuli in complex networks composed of another improved new neuron models which consider more real physical and biological effects (Lv et al., 2016; Lv and Ma, 2016; Gu and Pan, 2015; Gu et al., 2014) also seem to be interesting, which is left as a future work. We also considered the excitatory and the inhibitory synchronization separately. However, a neural circuit in the major parts of the brain is composed of both excitatory principal cells and inhibitory interneurons. Hence, it seems to be reasonable to consider a network consisting of both excitatory and inhibitory neurons. For this combined case, we also expect that our results would be largely valid, although more rich phenomena could occur via competition between excitation and inhibition. Stimulated excitatory (inhibitory) neurons are expected to make constructive (destructive) effects on non-stimulated excitatory or inhibitory neurons by causing external phase lockings (destroying original synchronization).

Acknowledgements This research was supported by the Basic Science Research Program through the National Research Foundation of Korea (NRF) funded by the Ministry of Education (Grant No. 20162007688).

Appendix: Statistical-mechanical spiking measure in the stimulated and the non-stimulated sub-populations

We measure the degree of population synchronization in each of the stimulated and the non-stimulated sub-populations in terms of a realistic statistical-mechanical spiking measure, based on the ISPSR kernel estimate $R_s^{(l)}(t)$ ($l = 1$ and 2 correspond to the stimulated and the non-stimulated cases, respectively) (Kim and Lim 2014). Population synchronization may be well visualized in the raster plot of spikes. For a synchronized case, spiking stripes or bursting bands (indicating population synchronization) appear successively in the raster plot, and the corresponding ISPSR kernel estimate $R_s^{(l)}(t)$ exhibits a regular oscillation. Each i th ($i = 1, 2, 3, \dots$) global cycle of $R_s^{(l)}(t)$ begins from its left minimum, passes the central maximum, and ends at the right minimum [also, corresponding to the beginning point of the next $(i + 1)$ th global cycle]; the 1st global cycle of $R_s^{(l)}(t)$ appears after transient times of 10^3 ms. Spikes which appear in the i th global cycle of $R_s^{(l)}(t)$ forms the i th stripe/band in the raster plot. To measure the degree of population synchronization in each of the stimulated ($l = 1$) and the non-stimulated ($l = 2$) sub-populations, a statistical-mechanical measure $M_s^{(l)}$, based on $R_s^{(l)}(t)$, was introduced by considering the occupation pattern and the pacing pattern of spikes in the stripes/bands (Kim and Lim 2014). The spiking measures $M_i^{(l)}$ of the i th stripe/band [appearing in the i th global cycle of $R_s^{(l)}(t)$] is defined by the product of the occupation degree $O_i^{(l)}$ of spikes (representing the density of the i th stripe/band) and the pacing degree $P_i^{(l)}$ of spikes (denoting the smearing of the i th stripe/band):

$$M_i^{(l)} = O_i^{(l)} \cdot P_i^{(l)}. \quad (14)$$

The occupation degrees $O_i^{(l)}$ in the i th stripe/band is given by the fractions of spiking neurons in the i th stripe/band:

$$O_i^{(l)} = \frac{N_i^{(l)}}{N}, \quad (15)$$

where $N_i^{(l)}$ is the number of spiking neurons in the i th stripe/band. For full synchronization with fully-occupied stripes/bands, $O_i^{(l)} = 1$, while for sparse synchronization with partially-occupied stripes/bands, $O_i^{(l)} < 1$. The pacing degree $P_i^{(l)}$ of spikes in the i th stripe/band can be determined in a statistical-mechanical way by taking into account their contributions to the macroscopic ISPSR kernel estimate $R_s^{(l)}(t)$. An instantaneous global phase $\Phi^{(l)}(t)$ of $R_s^{(l)}(t)$ was introduced via linear interpolation in

the two successive subregions forming global cycles (Kim and Lim 2014). The global phase $\Phi^{(l)}(t)$ between the left minimum (corresponding to the beginning point of the i th global cycle) and the central maximum is given by

$$\Phi^{(l)}(t) = 2\pi(i - 3/2) + \pi \left(\frac{t - t_i^{(l,min)}}{t_i^{(l,max)} - t_i^{(l,min)}} \right) \text{ for } t_i^{(l,min)} \leq t < t_i^{(l,max)}, \quad (16)$$

and $\Phi^{(l)}(t)$ between the central maximum and the right minimum [corresponding to the beginning point of the $(i + 1)$ th global cycle] is given by

$$\Phi^{(l)}(t) = 2\pi(i - 1) + \pi \left(\frac{t - t_i^{(l,max)}}{t_{i+1}^{(l,min)} - t_i^{(l,max)}} \right) \text{ for } t_i^{(l,max)} \leq t < t_{i+1}^{(l,min)}, \quad (17)$$

where $t_i^{(l,min)}$ is the beginning time of the i th ($i = 1, 2, 3, \dots$) global cycle of $R_s^{(l)}(t)$ [i.e., the time at which the left minimum of $R_s^{(l)}(t)$ appears in the i th global cycle], and $t_i^{(l,max)}$ is the time at which the maximum of $R_s^{(l)}(t)$ appears in the i th global cycle. Then, the contributions of the k th microscopic spikes in the i th stripe/band occurring at the times $t_k^{(l)}$ to $R_s^{(l)}(t)$ is given by $\cos \Phi_k^{(l)}$, where $\Phi_k^{(l)}$ are the global phases at the k th spiking time [i.e., $\Phi_k^{(l)} \equiv \Phi^{(l)}(t_k^{(l)})$]. Microscopic spikes make the most constructive (in-phase) contributions to $R_s^{(l)}(t)$ when the corresponding global phases $\Phi_k^{(l)}$ is $2\pi n$ ($n = 0, 1, 2, \dots$), while they make the most destructive (anti-phase) contribution to $R_s^{(l)}(t)$ when $\Phi_k^{(l)}$ is $2\pi(n - 1/2)$. By averaging the contributions of all microscopic spikes in the i th stripe/band to $R_s^{(l)}(t)$, we obtain the pacing degrees $P_i^{(l)}$ of spikes in the i th stripe/band:

$$P_i^{(l)} = \frac{1}{S_i^{(l)}} \sum_{k=1}^{S_i^{(l)}} \cos \Phi_k^{(l)} \quad (18)$$

where $S_i^{(l)}$ is the total number of microscopic spikes in the i th stripe/band. By averaging $M_i^{(l)}$ of Eq. (14) over a sufficiently large number $N_s^{(l)}$ of stripes/bands, we obtain the statistical-mechanical spiking measure $M_s^{(l)}$:

$$M_s^{(l)} = \frac{1}{N_s^{(l)}} \sum_{i=1}^{N_s^{(l)}} M_i^{(l)}. \quad (19)$$

Here, we follow 3×10^3 global cycles in each realization, and obtain the average occupation degree, the average pacing degree, and the average statistical-mechanical spiking measure via average over 30 (60) realizations for

the case of the non-stimulated (stimulated) sub-population. Here, more realizations are necessary for the stimulated case because the number $N_s (=50)$ of stimulated neurons is much less than that $(=950)$ of non-stimulated neurons.

References

- Batista CAS, Batista AM, de Pontes JAC, Viana RL, Lopes SR (2007) Chaotic phase synchronization in scale-free networks of bursting neuron. *Phys Rev E* 76:016218
- Batista CAS, Lopes SR, Viana RL, Batista AM (2010) Delayed feedback control of bursting synchronization in a scale-free neuronal network. *Neural Netw* 23:114–124
- Batista CAS, Viana RL, Ferrari FAS, Lopes SR, Batista AM, Coninck JCP (2013) Control of bursting synchronization in networks of Hodgkin–Huxley-type neurons with chemical synapses. *Phys Rev E* 87:042713
- Benabid AL, Chabardes S, Mitrofanis J, Pollak P (2009) Deep brain stimulation of the subthalamic nucleus for the treatment of Parkinson's disease. *Lancet Neurol* 8:67–81
- Brunel N, Hakim V (2008) Sparsely synchronized neuronal oscillations. *Chaos* 18:015113
- Brunel N, Wang XJ (2003) What determines the frequency of fast network oscillations with irregular neural discharges? I. Synaptic dynamics and excitation-inhibition balance. *J Neurophysiol* 90:415–430
- Bullmore E, Sporns O (2009) Complex brain networks: graph-theoretical analysis of structural and functional systems. *Nat Rev Neurosci* 10:186198
- Buzsáki G (2006) *Rhythms of the brain*. Oxford University Press, New York
- Buzsáki G, Geisler C, Henze DA, Wang XJ (2004) Interneuron diversity series: circuit complexity and axon wiring economy of cortical interneurons. *Trends Neurosci* 27:186–193
- Golomb D, Rinzel J (1994) Clustering in globally coupled inhibitory neurons. *Phys D* 72:259–282
- Gray CM (1994) Synchronous oscillations in neuronal systems: mechanisms and functions. *J Comput Neurosci* 1:11–38
- Gu H, Pan B (2015) A four-dimensional neuronal model to describe the complex nonlinear dynamics observed in the firing patterns of a sciatic nerve chronic constriction injury model. *Nonlinear Dyn* 81:2107–2126
- Gu H, Pan B, Chen G, Duan L (2014) Biological experimental demonstration of bifurcations from bursting to spiking predicted by theoretical models. *Nonlinear Dyn* 78:391–407
- Guare J (1990) *Six degrees of separation: a play*. Random House, New York
- Hamani C, Neimat J, Lozano AM (2006) Deep brain stimulation for the treatment of Parkinson's disease. *J Neural Transm Suppl* 70:393–399
- Hammond C, Bergman H, Brown P (2007) Pathological synchronization in Parkinson's disease: networks, models and treatments. *Trends Neurosci* 30:357–364
- Hodgkin AL (1948) The local electric changes associated with repetitive action in a non-medullated axon. *J Physiol* 107:165–181
- Ivanchenko MV, Osipov GV, Shalfeev VD, Kurths J (2004) Phase synchronization in ensembles of bursting oscillators. *Phys Rev Lett* 93:134101
- Izhikevich EM (2000) Neural excitability, spiking and bursting. *Int J Bifurc Chaos* 10:1171–1266
- Izhikevich EM (2003) Simple model of spiking neurons. *IEEE Trans Neural Netw* 14:1569–1572
- Izhikevich EM (2004) Which model to use for cortical spiking neurons? *IEEE Trans Neural Netw* 15:1063–1070
- Izhikevich EM (2007) *Dynamical systems in neuroscience*. MIT Press, Cambridge
- Izhikevich EM (2010) Hybrid spiking models. *Philos Trans R Soc A* 368:5061–5070
- Joris PX, Carney LH, Smith PH, Yin TCT (1994) Enhancement of neural synchronization in the anteroventral cochlear nucleus. I. Responses to tones at the characteristic frequency. *J Neurophysiol* 71:1022–1036
- Kim SY, Lim W (2013) Coupling-induced population synchronization in an excitatory population of subthreshold Izhikevich neurons. *Cogn Neurodyn* 7:495–503
- Kim SY, Lim W (2014) Realistic thermodynamic and statistical-mechanical measures for neural synchronization. *J Neurosci Methods* 226:161–170
- Kim SY, Lim W (2015a) Noise-induced burst and spike synchronizations in an inhibitory small-world network of subthreshold bursting neurons. *Cogn Neurodyn* 9:179–200
- Kim SY, Lim W (2015b) Effect of small-world connectivity on fast sparsely synchronized cortical rhythms. *Phys A* 421:109–123
- Kim SY, Kim Y, Hong DG, Kim J, Lim W (2012) Stochastic bursting synchronization in a population of subthreshold Izhikevich neurons. *J Korean Phys Soc* 60:1441–1447
- Lim W, Kim SY (2007) Characterization of stochastic spiking coherence in coupled neurons. *J Korean Phys Soc* 51:1427–1431
- Lim W, Kim SY (2011) Statistical-mechanical measure of stochastic spiking coherence in a population of inhibitory subthreshold neuron. *J Comput Neurosci* 31:667–677
- Longtin A (1995) Synchronization of the stochastic Fitzhugh–Nagumo equations to periodic forcing. *Nuovo Cimento D* 17:835–846
- Longtin A (2000) Stochastic aspects of neural phase locking to periodic signals. In: Kim S, Lee KJ, Sung W (eds) *Stochastic dynamics and pattern formation in biological and complex systems*. AIP, New York, pp 219–239
- Lv M, Ma J (2016) Multiple modes of electrical activities in a new neuron model under electromagnetic radiation. *Neurocomputing* 205:375–381
- Lv M, Wang C, Ren G, Ma J (2016) Model of electrical activity in a neuron under magnetic flow effect. *Nonlinear Dyn* 85:1479–1490
- Mathewson KE, Prudhomme C, Fabiani M, Beck DM, Lleras A, Gratton G (2012) Making waves in the stream of consciousness: entraining oscillations in EEG alpha and fluctuations in visual awareness with rhythmic visual stimulation. *J Cogn Neurosci* 24:2321–2333
- Milgram S (1967) The small world problem. *Psychol Today* 1:61–67
- Milton J, Jung P (eds) (2003) *Epilepsy as a dynamic disease*. Springer, Berlin
- Press WH, Teukolsky SA, Vetterling WT, Flannery BP (1992) *Numerical recipes in C: the art of scientific computing*, 2nd edn. Cambridge University Press, New York
- Rosenblum MG, Pikovsky AS (2004a) Controlling synchronization in an ensemble of globally coupled oscillators. *Phys Rev Lett* 92:114102
- Rosenblum MG, Pikovsky AS (2004b) Delayed feedback control of collective synchrony: an approach to suppression of pathological brain rhythms. *Phys Rev E* 70:041904
- San Miguel M, Toral R (2000) Stochastic effects in physical systems. In: Martinez J, Tiemann R, Tirapegui E (eds) *Instabilities and nonequilibrium structures VI*. Kluwer Academic Publisher, Dordrecht, pp 35–130

- Shimazaki H, Shinomoto S (2010) Kernel bandwidth optimization in spike rate estimation. *J Comput Neurosci* 29:171–182
- Sporns O (2011) *Netw brain*. MIT Press, Cambridge
- Strogatz SH (2001) Exploring complex networks. *Nature* 410:268–276
- Traub RD, Whittington MA (2010) *Cortical oscillations in health and diseases*. Oxford University Press, New York
- Uhlhaas PJ, Singer W (2006) Neural synchrony in brain disorders: relevance for cognitive dysfunctions and pathophysiology. *Neuron* 52:155–168
- Viana RL, Batista AM, Batista CAS, de Pontes JCA, dos S Silva FA, Lopes SR (2012) Bursting synchronization in networks with long-range coupling mediated by a diffusing chemical substance. *Commun Nonlinear Sci Numer Simul* 17:2924–2942
- Wang XJ (2003) Neural oscillations. In: Nadel L (ed) *Encyclopedia of cognitive science*. MacMillan, London, pp 272–280
- Wang XJ (2010) Neurophysiological and computational principles of cortical rhythms in cognition. *Physiol Rev* 90:1195–1268
- Watts DJ (2003) *Small worlds: the dynamics of networks between order and randomness*. Princeton University Press, Princeton
- Watts DJ, Strogatz SH (1998) Collective dynamics of small-world networks. *Nature* 393:440–442
- Will U, Berg E (2007) Brain wave synchronization and entrainment to periodic acoustic stimuli. *Neurosci Lett* 424:55–60